J. Fluid Mech. (2010), *vol.* 662, *pp.* 447–474.
doi:10.1017/S0022112010003307

Lift on a sphere moving near a wall in a parabolic flow

SAMIR YAHIAOUI[1] AND FRANÇOIS FEUILLEBOIS[2]†

[1]Laboratoire PMMH, CNRS UMR 7636 – ESPCI, 10 rue Vauquelin, 75231 Paris Cedex 05, France

[2]LIMSI-CNRS, UPR 3251, B.P. 133, 91403 Orsay Cedex, France

(Received 7 September 2009; revised 17 June 2010; accepted 17 June 2010;
first published online 6 September 2010)

The lift on a solid sphere moving along a wall in a parabolic shear flow is obtained as a regular perturbation problem for low Reynolds number when the sphere is in the inner region of expansion. Comprehensive results are given for the 10 terms of the lift, which involve the sphere translation and rotation, the linear and quadratic parts of the shear flow and all binary couplings. Based on very accurate earlier results of a creeping flow in bispherical coordinates, precise results for these lift terms are obtained for a large range of sphere-to-wall distances, including the lubrication region for sphere-to-wall gaps down to 0.01 of a sphere radius. Fitting formulae are also provided in view of applications. The migration velocity of an inertialess spherical particle is given explicitly, for a non-rotating sphere with a prescribed translation velocity and for a freely moving sphere in a parabolic shear flow. Values of the lift and migration velocity are in good agreement with earlier results whenever available.

Key words: low-Reynolds-number flows, particle/fluid flows, suspensions

1. Introduction

Particles carried by a viscous fluid along a wall may be subjected to a lift force normal to this wall. This lift force has various applications in chemical engineering processes. It is also important in analytical chemistry, e.g. for the field-flow-fractionation (FFF) technique, wherein particles pushed by the lift force reach streamlines of different velocities and are separated therefrom (Giddings 1978). We consider here the model of a rigid solid spherical particle moving in a shear flow along a solid plane wall. The particle is small enough for the particle Reynolds number to be low compared with unity. At leading order in the low Reynolds number, say order(0) for vanishing Reynolds number, the hydrodynamic force on the sphere is parallel to the wall, from the linearity of the Stokes equations of fluid motion (Bretherton 1962). At the next order, say order(1), a small fluid inertia provides a lift force normal to the wall.

Actually several Reynolds numbers based on the sphere radius a may be considered. For a sphere translating in a linear shear flow, relevant Reynolds numbers are $Re_V = aV/\nu_f$, where V is the fluid velocity relative to the sphere centre, and $Re_S = a^2\tilde{K}_S/\nu_f$, where $\tilde{K}_S$ is the shear rate. Here, ν_f denotes the fluid kinematic viscosity. Since the original works of Oseen (1914) and Proudman & Pearson (1957) for a translating sphere, and of Saffman (1965) for a moving sphere in a linear shear

† Email address for correspondence: francois.feuillebois@limsi.fr

flow, it has been well known that perturbation problems at order(1) are singular in an unbounded fluid. Since the 1950s and 1960s, such problems have been treated with the method of matched asymptotic expansions. On the other hand, for a wall-bounded flow, the problem may be regular at leading order, as shown by Cox & Brenner (1968). Indeed, when a wall is located in the inner region of expansion, at a distance ℓ from the sphere centre that is small compared with the Oseen radius a/Re_V, the translation problem at $O(Re_V)$ is regular. Likewise, the shear-flow problem at $O(\sqrt{Re_S})$ is regular when the wall distance is small compared with the Saffman distance $a/\sqrt{Re_S}$. There is a large body of literature on these singular and regular problems. For reviews, see, e.g., Feuillebois (1989, 2004).

We concentrate here on wall-bounded flows and regular problems. Cox & Brenner (1968) also proved that the lift force at order(1) may be obtained without solving the whole flow field, by using an improved version of the Lorentz reciprocity theorem (see, e.g., Happel & Brenner 1967 for the original theorem) coupling the orders(0) and (1). This technique was successfully applied by Ho & Leal (1974) to find the lift on neutrally buoyant spheres moving with a Poiseuille flow between parallel walls. They qualitatively obtained the effect observed by Segré & Silberberg (1961, 1962*a*,*b*), who found that particles carried by a Poiseuille flow in a pipe collect on a stream tube located around $0.6R$ from the cylinder axis, where R is the cylinder radius. Vasseur & Cox (1976) revised and improved the results of Ho & Leal (1974). An analogous calculation by Cox & Hsu (1977) applied the technique of Cox & Brenner (1968) to the case of a sphere near one wall. Like Vasseur & Cox (1976), they used the assumption that $a/\ell \ll 1$. Their results for a freely translating sphere that is either not rotating or freely rotating will be quoted later in this paper. The case of the lift on a small translating sphere near a wall was examined analytically and numerically by Cherukat & McLaughlin (1994), who derived expressions for the hydrodynamic force as a function of the distance from the wall. Their results are valid for $1.1 \leqslant \ell/a \leqslant 20$ and $-5 \leqslant Re_S/Re_V \leqslant 5$. The lift on a spherical particle attached to a wall in a linear shear flow was treated by Leighton & Acrivos (1987). Krishnan & Leighton (1995) generalized their results to the case where a sphere can move along the wall. All these results were obtained after solving regular perturbation problems, as in Ho & Leal (1974).

A better comparison with the experiment of Segré & Silberberg (1961, 1962*a*,*b*) was provided by later works involving a higher pipe flow Reynolds number, whereby the problem then is singular (see, e.g., Asmolov 1999), but this is out of the scope of the present paper. Other theoretical and numerical simulations that are not addressed in this study concern the lift force on drops and bubbles in shear flows (see, e.g., Legendre & Magnaudet 1997, 1998 and Magnaudet 2003).

The focus here is on a particle close to a wall in a parabolic shear flow (which has a linear and a quadratic part). The goal is to provide comprehensive results connecting earlier works and to complete data for a sphere in the lubrication region.

The formulation for order(0) and order(1) and the solution technique for order(1) are presented in § 2. Results for the lift force are given in § 3 and for the migration velocity and some trajectories in § 4. Finally, the conclusion and discussion are presented in § 5.

2. Problem formulation and solution technique

2.1. *Problem formulation*

In this subsection, we introduce the various flow fields and the problem expansion in low Reynolds number. Consider (figure 1) a solid spherical particle with radius a

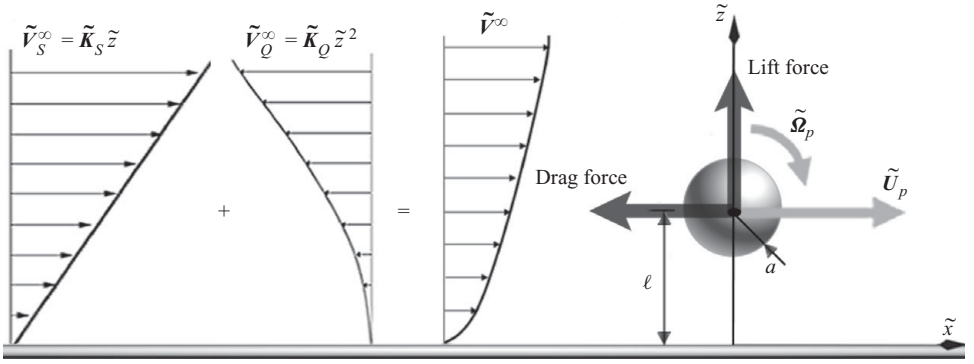

FIGURE 1. Particle moving in a parabolic flow near a wall, superimposing linear shear and quadratic shear flows.

centred at a distance ℓ from a solid plane wall. We use here a Cartesian coordinates system with $\tilde{x}, \tilde{y}$ along the wall and $\tilde{z}$ normal to it. Let $\boldsymbol{e}_x$, $\boldsymbol{e}_y$ and $\boldsymbol{e}_z$ be the unit vectors in these directions. The sphere is translating with a velocity $\tilde{\boldsymbol{U}}_p = \tilde{U}_p\boldsymbol{e}_x$ along the wall in the $\tilde{x}$ direction and rotating with a velocity $\tilde{\boldsymbol{\Omega}}_p = \tilde{\Omega}_p\boldsymbol{e}_y$ in the $\tilde{y}$ direction. The sphere is embedded in an ambient parabolic shear flow along $\tilde{x}$, which can be written with linear and quadratic parts as

$$\tilde{\boldsymbol{V}}^\infty = \tilde{\boldsymbol{V}}_S^\infty + \tilde{\boldsymbol{V}}_Q^\infty \quad \text{with} \quad \tilde{\boldsymbol{V}}_S^\infty = \tilde{K}_S\tilde{z}\boldsymbol{e}_x \quad \text{and} \quad \tilde{\boldsymbol{V}}_Q^\infty = \tilde{K}_Q\tilde{z}^2\boldsymbol{e}_x, \tag{2.1}$$

with dimensional constants $\tilde{K}_S$ and $\tilde{K}_Q$. This flow may represent the near-wall region in a two-dimensional Poiseuille flow between parallel walls separated by a distance H. In that case,

$$\tilde{K}_S = -\frac{H}{2\mu_f}\frac{\mathrm{d}\tilde{P}^\infty}{\mathrm{d}\tilde{x}} \quad \text{and} \quad \tilde{K}_Q = \frac{1}{2\mu_f}\frac{\mathrm{d}\tilde{P}^\infty}{\mathrm{d}\tilde{x}} = -\frac{\tilde{K}_S}{H}, \tag{2.2}$$

where μ_f is the fluid dynamic viscosity and $\mathrm{d}\tilde{P}^\infty/\mathrm{d}\tilde{x}$ is the pressure gradient. The flow (2.1) may also represent the first-order terms in an expansion in $\tilde{z}$ of a boundary-layer flow along a wall.

We denote by $\tilde{\boldsymbol{V}}$ the velocity of the flow field influenced by the presence of the sphere, or a perturbed flow. In a reference frame moving with the particle centre, the perturbed velocity field is written as $\tilde{\boldsymbol{V}} = \tilde{\boldsymbol{V}}^\infty - \tilde{\boldsymbol{U}}_p + \tilde{\boldsymbol{v}}$, where $\tilde{\boldsymbol{v}}$ denotes the perturbation velocity which is the unknown of this problem. Similarly, we define the perturbed and perturbation pressures $\tilde{P}$ and $\tilde{p}$, respectively. The boundary conditions for the perturbation velocity are as follows:

$$\left.\begin{aligned} &\tilde{\boldsymbol{v}} = \tilde{\boldsymbol{U}}_p + \tilde{\boldsymbol{\Omega}}_p \times \tilde{\boldsymbol{r}} - \tilde{\boldsymbol{V}}^\infty, && \text{on the sphere surface,}\\ &\tilde{\boldsymbol{v}} = 0, && \text{on the wall,}\\ &\tilde{\boldsymbol{v}} \to 0, && \text{at infinity.} \end{aligned}\right\} \tag{2.3}$$

Here, $\tilde{\boldsymbol{r}}$ denotes a vector connecting the sphere centre to a point on its surface. The velocities are normalized by a characteristic velocity V^* (which remains to be defined in each case), the pressures by $\mu_f V^*/a$ and lengths by a. The dimensionless quantities will be denoted without tilde ($\tilde{\cdot}$). The particle Reynolds number based on the sphere radius and velocity V^* is assumed to be small compared with unity:

$$Re = \frac{aV^*}{\nu_f} \ll 1. \tag{2.4}$$

This condition should be enforced with a significant V^*, typically $V^* = \max\{|\tilde{\boldsymbol{V}}_0^\infty - \tilde{\boldsymbol{U}}_p|, a|\tilde{K}_S|, a^2|\tilde{K}_Q|\}$, where $\tilde{\boldsymbol{V}}_0^\infty$ is the unperturbed velocity at the sphere centre. However, for a purely rotating sphere, $V^* = a|\tilde{\boldsymbol{\Omega}}_p|$.

The expansions of the dimensionless perturbation fluid velocity and pressure in terms of the Reynolds number are written as

$$\boldsymbol{v} = \boldsymbol{v}^{(0)} + Re\, \boldsymbol{v}^{(1)} + O(Re^2), \quad p = p^{(0)} + Re\, p^{(1)} + O(Re^2). \tag{2.5}$$

The dimensionless translation and rotation velocities of the sphere are expanded in the same way:

$$\boldsymbol{U}_p = \boldsymbol{U}_p^{(0)} + Re\, \boldsymbol{U}_p^{(1)} + O(Re^2), \quad \boldsymbol{\Omega}_p = \boldsymbol{\Omega}_p^{(0)} + Re\, \boldsymbol{\Omega}_p^{(1)} + O(Re^2). \tag{2.6}$$

Replacing p, $\boldsymbol{v}$, $\boldsymbol{U}_p$ and $\boldsymbol{\Omega}_p$ by their expansions in Re, the Navier–Stokes equations with boundary conditions (2.3), at order(0), yield

$$\Delta \boldsymbol{v}^{(0)} - \nabla p^{(0)} = 0, \tag{2.7a}$$

$$\nabla \cdot \boldsymbol{v}^{(0)} = 0, \tag{2.7b}$$

i.e. Stokes equations, with the boundary conditions

$$\left.\begin{array}{ll} \boldsymbol{v}^{(0)} = \boldsymbol{U}_p^{(0)} + \boldsymbol{\Omega}_p^{(0)} \times \boldsymbol{r} - \boldsymbol{V}^\infty, & \text{on the sphere surface,} \\ \boldsymbol{v}^{(0)} = 0, & \text{on the wall,} \\ \boldsymbol{v}^{(0)} \to 0, & \text{at infinity.} \end{array}\right\} \tag{2.8}$$

The bispherical coordinates system (η, ξ, ϕ) is a familiar tool to solve such problems (see, e.g., Appendix A in Happel & Brenner 1967). It is defined from the cylindrical coordinates $(\rho = \tilde{\rho}/a = \sqrt{\tilde{x}^2 + \tilde{y}^2}/a,\ \phi = \tan^{-1}(\tilde{y}/\tilde{x}),\ z = \tilde{z}/a)$ by (2.9)–(2.11) (see figure 2):

$$\rho = c\frac{\sin\eta}{\cosh\xi - \cos\eta}, \tag{2.9}$$

$$z = c\frac{\sinh\xi}{\cosh\xi - \cos\eta}, \tag{2.10}$$

$$c = \sqrt{\ell^2/a^2 - 1}, \tag{2.11}$$

where $(\eta, \xi, \phi) \in [0, \pi] \times [0, \alpha] \times [0, 2\pi]$. As shown figure 2, the wall is represented by $\xi = 0$ and the sphere by $\xi = \alpha$, with $\ell/a = \cosh\alpha$, where α is a positive constant.

2.2. *Various solutions for a sphere in Stokes flows*

Solutions using the bispherical coordinates were obtained for the translation and rotation of a sphere in the fluid at rest by O'Neill (1964) and for a sphere held fixed in a linear shear flow by Tözeren & Skalak (1977). Chaoui & Feuillebois (2003) reconsidered these problems with a technique providing a high accuracy, even in the lubrication region. In a similar way, Pasol, Sellier & Feuillebois (2006) treated the case of a sphere held fixed in a quadratic shear flow. Since the fluid velocity at order(0) is necessary for the calculation of the lift force at order(1), some details are provided in Appendix A.

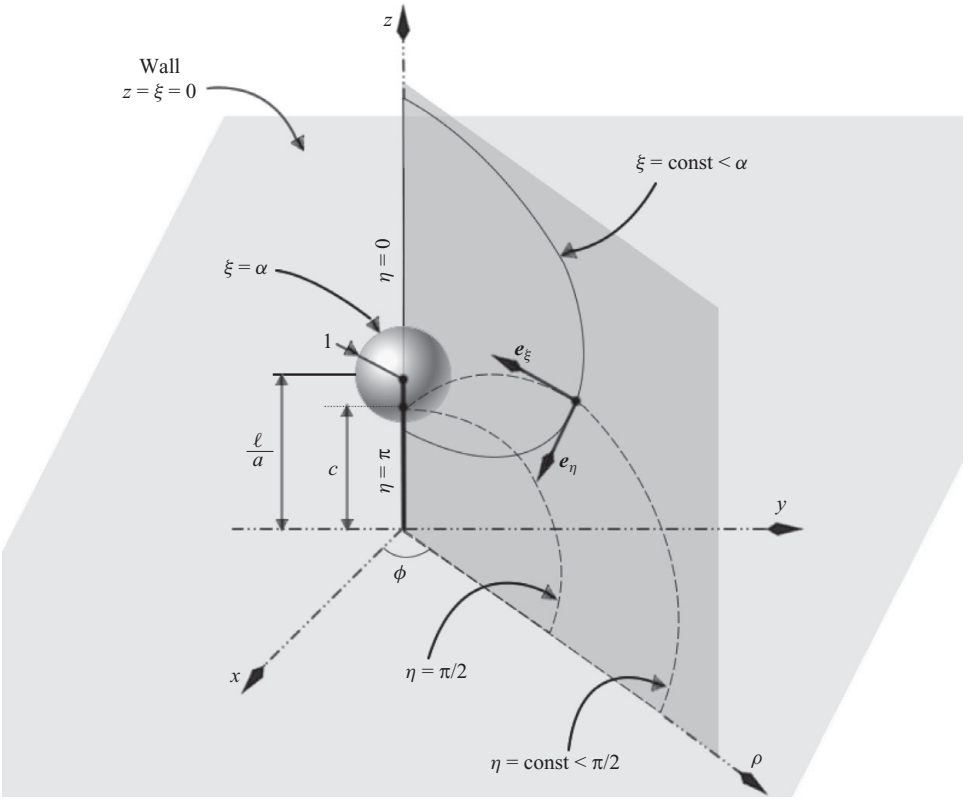

FIGURE 2. Bispherical coordinates.

Results for the hydrodynamic force $\mathscr{F}$ and torque $\mathscr{C}$ on the particle may be written in terms of friction factors in the various cases of

$$\text{translation: } \mathscr{F}_x^T = -6\pi a\mu_f \tilde{U}_p f_{xx}^T, \qquad \mathscr{C}_y^T = 8\pi a^2 \mu_f \tilde{U}_p c_{yx}^T, \tag{2.12}$$

$$\text{rotation: } \mathscr{F}_x^R = 6\pi a^2 \mu_f \tilde{\Omega}_p f_{xy}^R, \qquad \mathscr{C}_y^R = -8\pi a^3 \mu_f \tilde{\Omega}_p c_{yy}^R, \tag{2.13}$$

$$\text{a linear shear flow: } \mathscr{F}_x^S = 6\pi a\mu_f \ell \tilde{K}_S f_{xx}^S, \qquad \mathscr{C}_y^S = 4\pi a^3 \mu_f \tilde{K}_S c_{yx}^S, \tag{2.14}$$

$$\text{a quadratic shear flow: } \mathscr{F}_x^Q = 6\pi a\mu_f \ell^2 \tilde{K}_Q f_{xx}^Q, \qquad \mathscr{C}_y^Q = 8\pi a^3 \mu_f \ell \tilde{K}_Q c_{yx}^Q, \tag{2.15}$$

with obvious notation. All friction factors, denoted by f for the force and c for the torque, are functions of ℓ/a only. They are defined so that their limit is unity for $\ell/a \to \infty$ except for c_{yx}^T and f_{xy}^R, which vanish. The translation and rotation velocities of the particle are determined from its equations of motion, using these expressions for the values of $\mathscr{F}$ and $\mathscr{C}$. In the particular case of a freely translating and rotating sphere in a linear shear flow, $\mathscr{F}_x^R + \mathscr{F}_x^T + \mathscr{F}_x^S = 0$ and $\mathscr{C}_y^R + \mathscr{C}_y^T + \mathscr{C}_y^S = 0$ give $\tilde{U}_p = a\tilde{K}_S U_p^S$ and $\tilde{\Omega}_p = \tilde{K}_S \Omega_p^S$ with

$$U_p^S = \frac{\frac{\ell}{a} c_{yy}^R f_{xx}^S + \frac{1}{2} c_{yx}^S f_{xy}^R}{c_{yy}^R f_{xx}^T - c_{yx}^T f_{xy}^R}, \qquad \Omega_p^S = \frac{\frac{\ell}{a} c_{yx}^T f_{xx}^S + \frac{1}{2} c_{yx}^S f_{xx}^T}{c_{yy}^R f_{xx}^T - c_{yx}^T f_{xy}^R}, \tag{2.16}$$

whereas in a quadratic shear flow, $\mathscr{F}_x^R + \mathscr{F}_x^T + \mathscr{F}_x^Q = 0$ and $\mathscr{C}_y^R + \mathscr{C}_y^T + \mathscr{C}_y^Q = 0$ give $\tilde{U}_p = a^2 \tilde{K}_Q U_p^Q$ and $\tilde{\Omega}_p = a\tilde{K}_Q \Omega_p^Q$ with

$$U_p^Q = \frac{\left(\frac{\ell}{a}\right)^2 c_{yy}^R f_{xx}^Q + \frac{\ell}{a} c_{yx}^Q f_{xy}^R}{c_{yy}^R f_{xx}^T - c_{yx}^T f_{xy}^R}, \qquad \Omega_p^Q = \frac{\left(\frac{\ell}{a}\right)^2 c_{yx}^T f_{xx}^Q + \frac{\ell}{a} c_{yx}^Q f_{xx}^T}{c_{yy}^R f_{xx}^T - c_{yx}^T f_{xy}^R}. \tag{2.17}$$

Superimposing the linear and quadratic shear flows (see (2.1)), the dimensional translation and rotational velocities of a freely moving sphere are

$$\tilde{U}_p = a\tilde{K}_S U_p^S + a^2 \tilde{K}_Q U_p^Q, \tag{2.18a}$$

$$\tilde{\Omega}_p = \tilde{K}_S \Omega_p^S + a\tilde{K}_Q \Omega_p^Q. \tag{2.18b}$$

2.3. *Solution technique for the inertial lift force*

At next order in Reynolds number, the Navier–Stokes equations and boundary conditions yield

$$\left.\begin{aligned} \nabla \cdot \boldsymbol{v}^{(1)} &= 0, \\ \Delta \boldsymbol{v}^{(1)} - \nabla p^{(1)} &= \boldsymbol{f}, \end{aligned}\right\} \tag{2.19}$$

where

$$\boldsymbol{f} = \boldsymbol{v}^{(0)} \cdot \nabla \boldsymbol{v}^{(0)} + \boldsymbol{v}^{(0)} \cdot \nabla \boldsymbol{V}^{\infty} + (\boldsymbol{V}^{\infty} - \boldsymbol{U}_p) \cdot \nabla \boldsymbol{v}^{(0)}, \tag{2.20}$$

with the boundary conditions

$$\left.\begin{aligned} \boldsymbol{v}^{(1)} &= \boldsymbol{U}_p^{(1)} + \boldsymbol{\Omega}_p^{(1)} \times \boldsymbol{r}, && \text{on the sphere surface,} \\ \boldsymbol{v}^{(1)} &= 0, && \text{on the wall,} \\ \boldsymbol{v}^{(1)} &\to 0, && \text{at infinity.} \end{aligned}\right\} \tag{2.21}$$

Here, the particle is assumed to be close enough to the wall, or the Reynolds number small enough, for the wall to be in the inner region of expansion $\ell/a \ll (1/Re, 1/\sqrt{Re_S})$.

The dimensionless force on the sphere, using the reference $a\mu_f V^*$, is obtained as an expansion: $\boldsymbol{F} = \boldsymbol{F}^{(0)} + Re\,\boldsymbol{F}^{(1)} + O(Re^2)$. As seen above, $\boldsymbol{F}^{(0)}$ is a drag force along the wall. The force $\boldsymbol{F}^{(1)}$ contains a correction to the drag plus a lift force which is perpendicular to the ambient flow relative to the sphere, and thus is normal to the wall. This study is concerned with the calculation of this lift force, say $F_z^{(1)}$, which has various applications, e.g. for separation techniques (see § 1). To obtain $F_z^{(1)}$, calculating the whole flow field $(\boldsymbol{v}^{(1)}, p^{(1)})$ is unnecessary. It is sufficient to use a variation of the Lorentz reciprocity theorem proposed by Cox & Brenner (1968) and exploited by Ho & Leal (1974). This approach provides the relationship

$$F_z^{(1)} - 6\pi D_z U_{pz}^{(1)} = -\int_{V_f} \boldsymbol{f} \cdot \boldsymbol{w}\, \mathrm{d}V, \tag{2.22}$$

where V_f is the fluid domain, $U_{pz}^{(1)}$ is the (order(1)) migration velocity in the z direction of an inertialess freely moving particle, $\boldsymbol{w}$ is the Stokes flow velocity due to a sphere moving with unit velocity perpendicular to the wall and $-D_z$ is the drag force on this moving sphere. The solution for D_z was obtained independently by Brenner (1961) and Maude (1961) as a series in bispherical coordinates. It is valid for non-zero gaps. Typically, thousands of terms are needed for small gaps. Alternatively, the second-order expansion for small gaps by Cox & Brenner (1967) might be sufficient,

depending on the required precision. Now, we may consider two particular cases:

(*a*) The particle velocity $\boldsymbol{U}_p$ is imposed, so that $\boldsymbol{U}_p = \boldsymbol{U}_p^{(0)}$ and $\boldsymbol{U}_p^{(1)} = 0$. Then the dimensionless lift force can simply be expressed in terms of the velocity field at order(0) as

$$F_z = -Re \int_{V_f} \boldsymbol{f} \cdot \boldsymbol{w} \, \mathrm{d}V = -ReL. \tag{2.23}$$

(*b*) The inertialess particle is moving freely; then, from the zero-net-force condition we obtain the dimensionless migration velocity:

$$U_{\boldsymbol{m}} = Re\, U_{pz}^{(1)} = \frac{Re}{6\pi D_z} \int_{V_f} \boldsymbol{f} \cdot \boldsymbol{w} \, \mathrm{d}V = \frac{Re}{6\pi D_z} L. \tag{2.24}$$

A discussion about particle inertia is appropriate here. Since the particle velocity along z is of order $O(Re)$, fluid inertia due to this motion is $O(Re^2)$ and is thus negligible. As for particle inertia, it is characterized by a Stokes number $Sk = \tau_p/\tau_f$, ratio of the particle characteristic time $\tau_p = m_p/(6\pi a \mu_f)$, where m_p is the particle mass, to the ambient flow characteristic time $\tau_f = a/V^*$, giving $Sk \sim (\rho_p/\rho_f)Re$.

In a liquid, the ratio of particle to fluid density, ρ_p/ρ_f, is of order unity, so that $Sk \sim Re \ll 1$. More precisely, the particle equation of motion for translation in the direction normal to the wall, in terms of the dimensionless position $Z = \ell/a$ and time $t = \tilde{t}/\tau_f$ (where $\tilde{t}$ is the dimensional time), is

$$\frac{4\pi}{3} Re \frac{\rho_p}{\rho_f} \frac{\mathrm{d}Z}{\mathrm{d}t} + 6\pi D_z \frac{\mathrm{d}Z}{\mathrm{d}t} + ReL(Z) = 0. \tag{2.25}$$

Balancing the drag force (the second term) and the lift force (the third term) gives the time scaling $t \sim 1/Re$. For $\rho_p/\rho_f = O(1)$, particle inertia represented by the first term is negligible for the largest part of the time, $t \sim 1/Re$.

On the other hand, for solid particles in a gas, $\rho_p/\rho_f \gg 1$; then in some conditions, Sk might be of order unity so that particle inertia would be significant. In that case, the particle equations of motion for translation and rotation would have to be solved. In the equation of motion for rotation, there are inertial corrections to the torque which are not considered here. This problem of particles with $\rho_p/\rho_f \gg 1$ giving a significant particle inertia is out of the scope of the present paper.

We recall that in (2.23) and (2.24), $\boldsymbol{f}$ is given by (2.20), in which $\boldsymbol{v}^{(0)}$ is very accurately calculated with the method of bispherical coordinates. As for $\boldsymbol{w}$, the analytical solution of Brenner (1961) and Maude (1961) as a series is useful for our purpose of obtaining accurate results even down to the lubrication region. Details are given below in § 2.4.

It can be verified that the problem is of regular perturbation. Indeed, given the rapid decay of $\boldsymbol{f}$ and $\boldsymbol{w}$ at infinity, the integral over the semi-infinite domain V_f is convergent, unlike for the case of a sphere immersed in an infinite domain which would lead to the Whitehead paradox. This is because the fluid velocity due to a translating sphere in an unbounded fluid decays like $1/r$ whereas this decay is more rapid here because of the image of the sphere in the wall (Cox & Brenner 1968). Details of the behaviours of $\boldsymbol{f}$ and $\boldsymbol{w}$ at infinity are given in Appendix C (following the details concerning $\boldsymbol{f}$ in Appendix B).

The perturbation velocity $\boldsymbol{v}^{(0)}$, i.e. the solution of (2.7) and (2.8), is a linear combination of the following perturbation flows: $\boldsymbol{v}_T$ and $\boldsymbol{v}_R$ for a translating, respectively rotating, sphere in a fluid at rest; $\boldsymbol{v}_S$ and $\boldsymbol{v}_Q$ for a fixed sphere in a linear, respectively quadratic, shear flow parallel to the wall. Therefore, the general

solution is written as

$$\boldsymbol{v}^{(0)} = T_S \boldsymbol{v}_S + T_Q \boldsymbol{v}_Q + T_R \boldsymbol{v}_R + T_T \boldsymbol{v}_T, \tag{2.26}$$

where T_T, T_R, T_S, T_Q are dimensionless ratios given by

$$T_T = \frac{\tilde{U}_p}{V^*}, \quad T_R = \frac{a\tilde{\Omega}_p}{V^*}, \quad T_S = \frac{a\tilde{K}_S}{V^*}, \quad T_Q = \frac{a^2\tilde{K}_Q}{V^*}. \tag{2.27}$$

After substitution of $\boldsymbol{v}^{(0)}$ in the expression (2.20) of $\boldsymbol{f}$, we find

$$L = T_S^2 L_S + T_Q^2 L_Q + T_R^2 L_R + T_T^2 L_T + T_S T_Q L_{SQ} + T_S T_R L_{SR} + T_S T_T L_{ST} + T_Q T_R L_{QR} + T_Q T_T L_{QT} + T_R T_T L_{RT}, \tag{2.28}$$

with

$$L_S = \int_{V_f} \left(\boldsymbol{v}_S \cdot \nabla \boldsymbol{V}_S^\infty + \left(\boldsymbol{v}_S + \boldsymbol{V}_S^\infty\right) \cdot \nabla \boldsymbol{v}_S\right) \cdot \boldsymbol{w} \, \mathrm{d}V, \quad L_T = \int_{V_f} ((\boldsymbol{v}_T - \boldsymbol{e}_x) \cdot \nabla \boldsymbol{v}_T) \cdot \boldsymbol{w} \, \mathrm{d}V, \tag{2.29}$$

$$L_{SR} = \int_{V_f} \left(\boldsymbol{v}_R \cdot \nabla\left(\boldsymbol{v}_S + \boldsymbol{V}_S^\infty\right) + \left(\boldsymbol{v}_S + \boldsymbol{V}_S^\infty\right) \cdot \nabla \boldsymbol{v}_R\right) \cdot \boldsymbol{w} \, \mathrm{d}V, \quad L_R = \int_{V_f} (\boldsymbol{v}_R \cdot \nabla \boldsymbol{v}_R) \cdot \boldsymbol{w} \, \mathrm{d}V, \tag{2.30}$$

$$L_{ST} = \int_{V_f} \left(\boldsymbol{v}_T \cdot \nabla\left(\boldsymbol{v}_S + \boldsymbol{V}_S^\infty\right) + \left(\boldsymbol{v}_S + \boldsymbol{V}_S^\infty\right) \cdot \nabla \boldsymbol{v}_T - \boldsymbol{e}_x \cdot \nabla \boldsymbol{v}_S\right) \cdot \boldsymbol{w} \, \mathrm{d}V, \tag{2.31}$$

$$L_{RT} = \int_{V_f} (\boldsymbol{v}_R \cdot \nabla \boldsymbol{v}_T + (\boldsymbol{v}_T - \boldsymbol{e}_x) \cdot \nabla \boldsymbol{v}_R) \cdot \boldsymbol{w} \, \mathrm{d}V, \tag{2.32}$$

$$L_{SQ} = \int_{V_f} \left(\left(\boldsymbol{v}_S + \boldsymbol{V}_S^\infty\right) \cdot \nabla \boldsymbol{v}_Q + \left(\boldsymbol{v}_Q + \boldsymbol{V}_Q^\infty\right) \cdot \nabla \boldsymbol{v}_S + \boldsymbol{v}_Q \cdot \nabla \boldsymbol{V}_S^\infty + \boldsymbol{v}_S \cdot \nabla \boldsymbol{V}_Q^\infty\right) \cdot \boldsymbol{w} \, \mathrm{d}V. \tag{2.33}$$

The expressions of L_Q, L_{QR} and L_{QT} are obtained in a similar way, by replacing $\boldsymbol{v}_S$ and $\boldsymbol{V}_S^\infty$ by the velocities $\boldsymbol{v}_Q$ and $\boldsymbol{V}_Q^\infty$ of a quadratic flow in the above expressions of L_S, L_{SR} and L_{ST}.

In dimensional form, the lift force is $\mathscr{F} = \rho_f a^2 V^{*2} L$, where ρ_f is the fluid density, so that the arbitrary V^* cancels out as it should.

2.4. *Numerical calculation of integrals*

The various terms of the integrals appearing in (2.28) were derived in bispherical coordinates. Some details are given in Appendix B. The various integrals in (2.28) were then calculated numerically with a high accuracy for a wide range of sphere-to-wall distance ℓ/a, down to the lubrication region $\ell/a - 1 \ll 1$. In this last case, the order(0) velocities vary fast in the small gap between the sphere and the wall. The solutions in bispherical coordinates for these velocities then need an increasingly large number (typically thousands) of terms for decreasing $\ell/a - 1$. The velocity $\boldsymbol{w}$ for the motion normal to the wall was calculated using the series solutions of Brenner (1961) and Maude (1961). The other terms for asymmetric sphere motions were calculated using the results of Chaoui & Feuillebois (2003) and Pasol *et al.* (2006), who used an explicit rapid method for solving with a high accuracy the recurrence relationship giving coefficients in the series (see Appendix A for these series). The counterpart is that a large number of digits have to be used to avoid the accumulation of round-off errors generated by successive iterations. For this purpose, calculations were performed with the Maple™ symbolic language, adjusting the number of digits

for a prescribed accuracy. In the Maple™ code, the calculation of the volume integrals (2.28) was enclosed in a loop in which the number of digits was increased, until the obtained result for a prescribed accuracy did not depend any more on the number of digits. Practically, between 30 and 120 digits were necessary, depending on the case considered. For the integration itself, we used the Gauss–Kronrod technique. Results were compared with those obtained with the two-dimensional Richardson–Romberg and Gauss–Legendre techniques (see, e.g., Kythe & Schferkotter 2004 for a description of these techniques). The number of points in the integration was 15–21, depending on the sphere position. For example, for the case L_S, obtaining a 10^{-16} precision at a gap $\ell/a - 1 = 10^{-2}$ required typically 120 digits, 1284 terms in the series and 21 integration points. For $\ell/a - 1 \leqslant 0.01$, numerical values were practically difficult to obtain since the calculation time in Maple™ was typically several weeks on a standard PC.

3. Results for the lift force

This section provides numerical results for the 10 terms in the expression (2.28) of the dimensionless lift force in a wide range of sphere-to-wall distances. The precise numerical values found for each single elementary flow are first presented in table 1. These data are then compared with earlier results whenever available. Formulae fitting the numerical results for the lift force are provided for each elementary flow in terms of the wall-to-particle distance. The case of a sphere held fixed in shear flows is in § 3.1 and those of a rotating and translating sphere in a fluid at rest are in § 3.2. Finally, § 3.3 presents the terms which arise when sphere motions are coupled with ambient flows.

3.1. *Sphere held fixed in linear and quadratic shear flows*

For a sphere at rest, the velocity fields $\boldsymbol{v}_R$, $\boldsymbol{v}_T$ and their gradients are set to zero in the expression (2.28) giving $\boldsymbol{v}^{(0)}$. The integrals L_R, L_T, L_{SR}, L_{ST}, L_{QR}, L_{QT} and L_{RT} then vanish.

In the case of a linear shear flow, the dimensional lift force is eventually written as $\tilde{F}_L = \rho a^4 \tilde{K}_S^2 L_S$. Figure 3 shows the evolution of the normalized lift force L_S with the particle-to-wall distance ℓ/a. Among earlier works, calculations of Cherukat & McLaughlin (1994) are those that better reflect the lift force near the wall, in the range $\ell/a \geqslant 1.1$. In the limit case of a sphere in contact with the wall, $\ell/a = 1$, Krishnan & Leighton (1995) obtained the value $L_S = 9.257$. It is observed in the insets of figure 3 that our values of the lift force for ℓ/a in the interval $[1.1, 3]$ are close to those of Cherukat & McLaughlin (1994) but slightly less. For ℓ/a in the interval $[3, 10]$, our values are between those of Cherukat & McLaughlin (1994) and Cox & Hsu (1977). Our precise results resolve here the discrepancy between those earlier data. For positions ℓ/a above 10, our results confirm the values proposed by Cox & Hsu (1977). With our method, we could even obtain values of the lift force for dimensionless gaps $\ell/a - 1$ in the interval $[0.01, 0.1]$.

A quadratic shear flow usually occurs in combination with a linear shear flow. Consider the case where the sphere is fixed in a parabolic flow. The lift force is given by the general relationship (2.28) with $U_p = \Omega_p = 0$. We choose here $V^* = a\tilde{K}_S$. The lift force is plotted in figure 4 versus ℓ/a for various values of H/a and compared with that obtained for the linear shear flow. When the sphere is close to the wall, at $\ell/a = 1.05$, in the case of a linear shear flow, the lift force takes the value of 10.142, whereas in the case of a parabolic flow, it varies from 9.2525 for $H = 100a$ to 10.124 for $H = 5000a$. The lift force vanishes at some distance from the wall. For example,

ℓ/a	L_S	L_{SQ}	L_{SR}	L_{ST}	L_Q	L_{QR}	L_{QT}	L_{RT}	L_R	L_T
100	50363.67	2.359×10^7	5979.724	−566.426	1.855×10^9	24715.47	-1.142×10^5	−2.456	8.90×10^{-5}	1.771
20	2026.330	1.815×10^5	236.217	−117.975	2.838×10^6	978.101	−4470.540	−2.456	0.0022	1.777
15	1146.476	7.707×10^4	130.770	−90.318	9.055×10^5	547.219	−2651.390	−2.444	0.0039	1.780
10	516.623	2.349×10^4	56.114	−62.674	1.855×10^5	238.771	−1310.936	−2.417	0.0088	1.785
5	135.661	3354.412	12.688	−34.652	1.378×10^5	52.042	−407.616	−2.323	0.0343	1.791
4	89.228	1851.667	7.7858	−28.854	6242.164	29.361	−277.917	−2.270	0.0523	1.789
3	52.710	888.072	4.132	−22.884	2347.287	11.716	−166.753	−2.177	0.0885	1.780
2	26.109	339.662	1.660	−16.662	655.029	−0.644	−74.552	−1.987	0.178	1.756
1.5	16.503	181.899	0.806	−13.477	285.512	−4.478	−27.921	−1.791	0.282	1.735
1.1	10.702	96.646	0.193	−11.179	125.700	−5.549	27.015	−1.228	0.457	1.731
1.07	10.385	92.687	0.108	−11.049	117.357	−5.563	37.836	−1.023	0.477	1.729
1.05	10.142	90.136	0.061	−10.967	102.932	−5.561	47.218	−0.794	0.491	1.728
1.01	9.451	85.283	0.018	−10.814	–	–	64.419	−0.139	0.526	1.748

TABLE 1. Values of the 10 integrals in (2.28) which give the dimensionless lift force as a function of the normalized position of the sphere centre, ℓ/a.

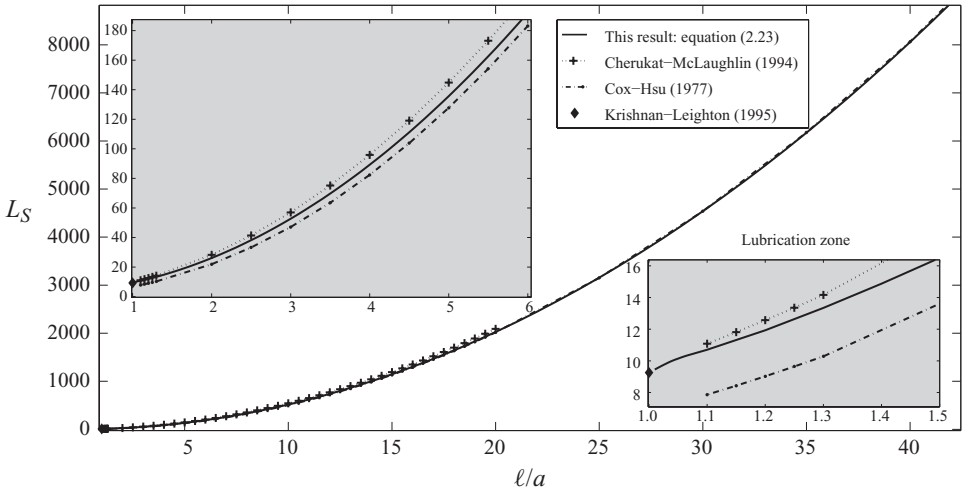

FIGURE 3. Lift force on a fixed sphere in a linear shear flow and comparison with the results of Cherukat & McLaughlin (1994), Cox & Hsu (1977) and Krishnan & Leighton (1995).

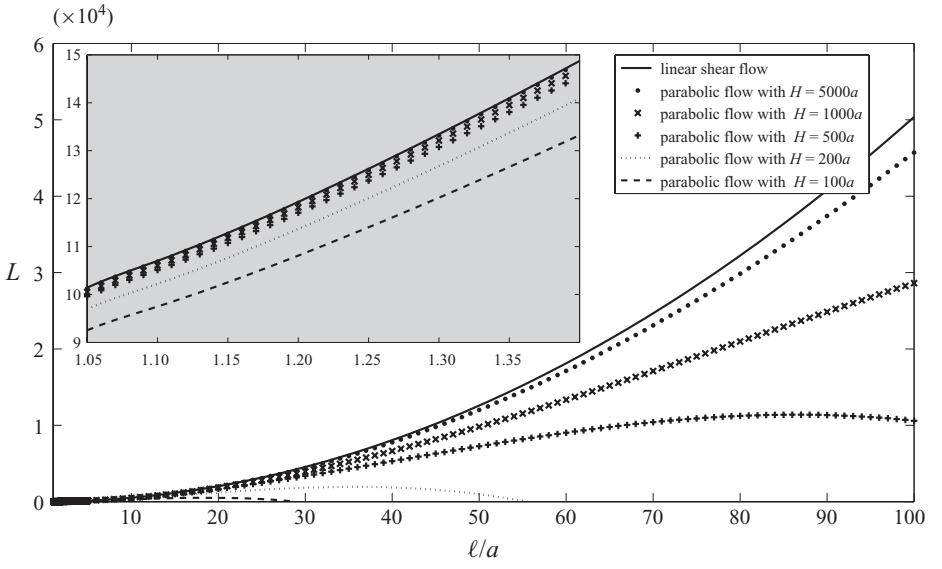

FIGURE 4. Lift force on a fixed sphere in a parabolic flow for various values of H/a and a comparison with the linear shear flow.

in the case $H = 200a$, it vanishes for $\ell/a = 55$, that is $\ell/H = 0.275$. This value is exact for an ambient flow involving a pressure gradient and a shear near a single wall. For two walls separated by the distance H, this is clearly an approximation. For a handy use of our numerical results, a sample of which is presented in table 1, we propose the following fitting formula for the normalized lift force on a sphere held fixed in a linear shear flow, which is valid for $Re \ll 1$ and all distances $1.01 \leqslant \ell/a \leqslant 100$:

$$\ln L_S = \frac{2.0172\lambda^5 + 3.4562\lambda^4 + 3.9608\lambda^3 + 2.6728\lambda^2 - 0.15728\lambda + 0.01386}{\lambda^4 + 0.96328\lambda^3 + 1.264\lambda^2 - 0.07648\lambda + 0.006228}, \qquad (3.1)$$

with $\lambda = \ln(\ell/a)$.

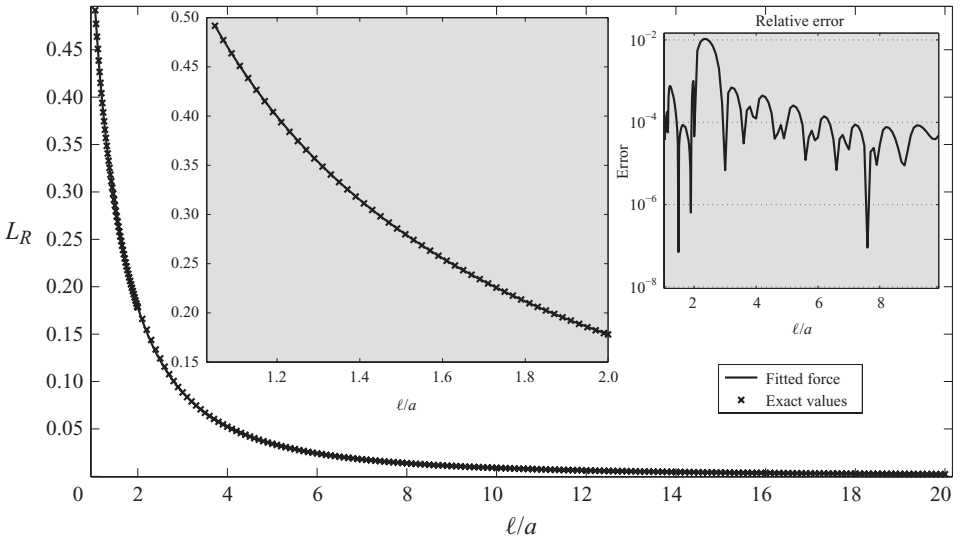

FIGURE 5. Exact solution and fitted formula (see (3.5)) for the lift force on a rotating sphere in a fluid at rest. Insets show a zoom on the near-wall region and the relative error.

In the case of a quadratic shear flow, results for the normalized lift force are fitted by

$$\ln L_Q = \begin{cases} \dfrac{191.2\lambda^4 + 13.91\lambda^3 + 332.2\lambda^2 - 76.63\lambda + 376}{\lambda^3 + 87.64\lambda^3 - 61.84\lambda + 82.28}, & \text{if } \dfrac{\ell}{a} < 2, \\ \dfrac{3.639\lambda^4 + 13.64\lambda^3 + 28.87\lambda^2 + 27.38\lambda - 57.25}{\lambda^3 + 1.408\lambda^2 + 12.13\lambda - 12.35}, & \text{if } \dfrac{\ell}{a} \geqslant 2. \end{cases} \tag{3.2}$$

For the integral coupling a quadratic flow and a linear shear flow, we obtain the fitting

$$\ln L_{SQ} = \begin{cases} \dfrac{20.44\lambda^5 + 8.227\lambda^4 + 16.24\lambda^3 + 13.69\lambda^2 + 20.4\lambda + 24.19}{\lambda^5 + 0.1743\lambda^4 + 7.395\lambda^3 - 1.543\lambda^2 + 3.093\lambda + 5.455}, & \text{if } \dfrac{\ell}{a} < 2, \\ \dfrac{2.965\lambda^5 - 4.143\lambda^4 + 21.64\lambda^3 + 53.86\lambda^2 + 68.25\lambda + 81.7}{\lambda^4 + 10.34\lambda^3 + 6.86\lambda^2 + 6.86\lambda + 18.64}, & \text{if } \dfrac{\ell}{a} \geqslant 2. \end{cases} \tag{3.3}$$

These formulae fit our precise results with a 0.1 % accuracy.

3.2. *Translating and rotating sphere in a fluid at rest*

This subsection concerns a sphere with a pure rotating motion, a pure translating motion and the coupling between rotation and translation in a fluid at rest at infinity. For these configurations, cancelling out the contributions of the linear and quadratic shear flows gives the following expression for the dimensional lift force:

$$\tilde{F}_L = \rho a \left[(a\tilde{\Omega}_p)^2 L_R + (\tilde{U}_p)^2 L_T + (a\tilde{\Omega}_p \tilde{U}_p) L_{RT} \right]. \tag{3.4}$$

The numerical values of the integrals L_R, L_T and L_{RT} are displayed in table 1 and are, respectively, represented in figures 5, 6 and 7. For pure translation, our results

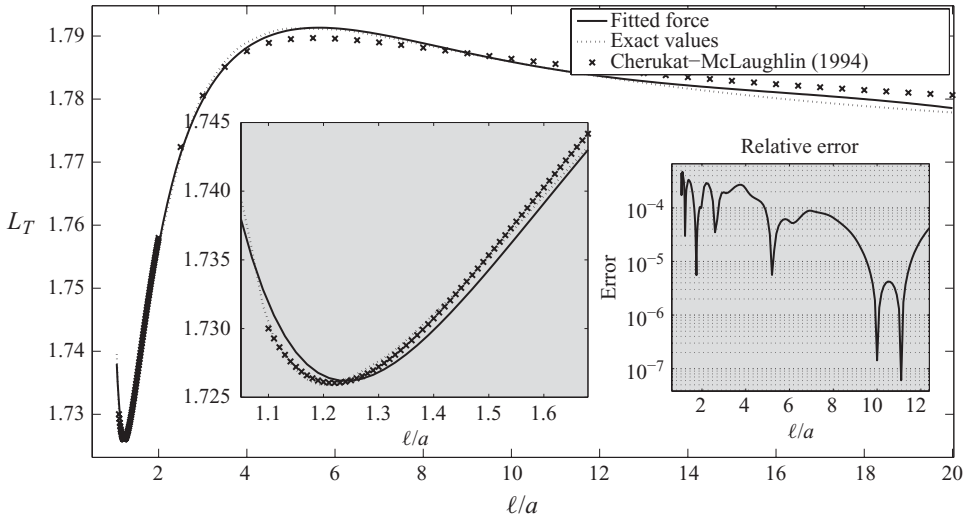

FIGURE 6. Exact solution and fitted formula (see (3.6)) for the lift force on a translating sphere in a fluid at rest and comparison with the results of Cherukat & McLaughlin (1994). Insets show a zoom on the near-wall region and the relative error.

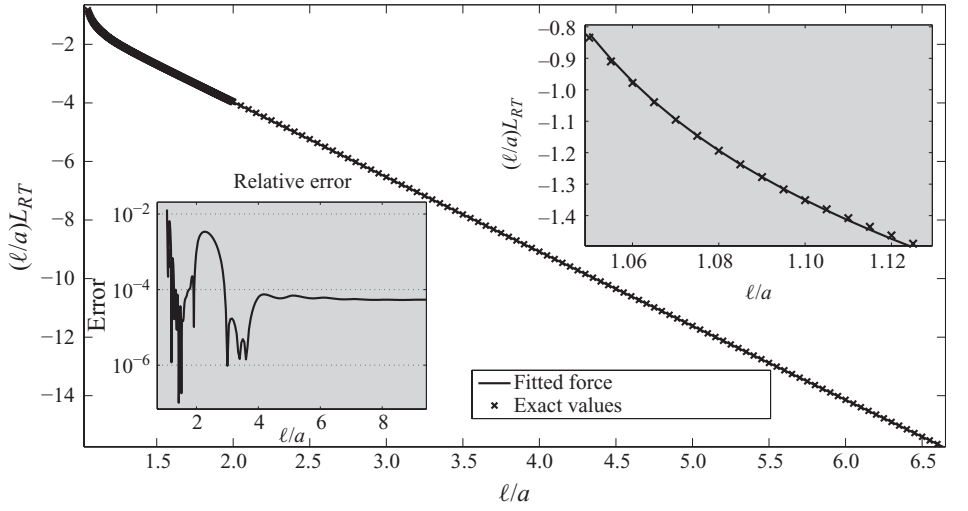

FIGURE 7. Exact solution and fitted formula (see (3.7)) for the lift force coupling term for a rotating and translating sphere in a fluid at rest. Insets show a zoom on the near-wall region and the relative error.

are in good agreement with those of Cherukat & McLaughlin (1994). By comparison, the value obtained by Cox & Hsu (1977) is $L_T = 18\pi/32 \simeq 1.767$.

Fitting formulae in the range $1.01 \leqslant \ell/a \leqslant 100$ are as follows.

(i) For a rotating sphere:

$$\ln L_R = \frac{-1.984\lambda^5 + 12.8\lambda^4 - 23.08\lambda^3 + 17.48\lambda^2 - 26.73\lambda - 14.17}{\lambda^4 - 6.618\lambda^3 + 13.17\lambda^2 - 14.12\lambda + 22.45}. \tag{3.5}$$

(ii) For a translating sphere:

$$\frac{\ell}{a}L_T = \frac{1.77\left(\frac{\ell}{a}\right)^4 + 14.48\left(\frac{\ell}{a}\right)^3 + 45.52\left(\frac{\ell}{a}\right)^2 - 42.67\left(\frac{\ell}{a}\right) + 9.243}{\left(\frac{\ell}{a}\right)^3 + 8.14\left(\frac{\ell}{a}\right)^2 + 23.59\left(\frac{\ell}{a}\right) - 16.54}. \tag{3.6}$$

(iii) For the rotation–translation coupling:

$$\frac{\ell}{a}L_{RT} = \begin{cases} \dfrac{-2.48\left(\frac{\ell}{a}\right)^4 + 8.394\left(\frac{\ell}{a}\right)^3 - 10.27\left(\frac{\ell}{a}\right)^2 + 5.265\left(\frac{\ell}{a}\right) - 0.9147}{\left(\frac{\ell}{a}\right)^3 - 3.002\left(\frac{\ell}{a}\right)^2 + 3.005\left(\frac{\ell}{a}\right) - 1.003}, & \text{if } \dfrac{\ell}{a} < 2, \\ \dfrac{-2.487\left(\frac{\ell}{a}\right)^4 - 324.5\left(\frac{\ell}{a}\right)^3 - 149.5\left(\frac{\ell}{a}\right)^2 + 1802\left(\frac{\ell}{a}\right) - 856.2}{\left(\frac{\ell}{a}\right)^3 + 130.7\left(\frac{\ell}{a}\right)^2 + 87.02\left(\frac{\ell}{a}\right) - 582.2}, & \text{if } \dfrac{\ell}{a} \geqslant 2. \end{cases} \tag{3.7}$$

3.3. *Coupling sphere motion with ambient flows*

Various coupling terms appear when the sphere is rotating and translating in ambient shear flows. We propose here fitting formulae for these lift force terms.

(i) Coupling shear flow and rotating sphere:

$$\frac{a}{\ell}L_{SR} = \begin{cases} \dfrac{0.5092\left(\frac{\ell}{a}\right)^4 - 1.775\left(\frac{\ell}{a}\right)^3 + 2.127\left(\frac{\ell}{a}\right)^2 - 0.9416\left(\frac{\ell}{a}\right) + 0.08043}{\left(\frac{\ell}{a}\right)^5 + 112700\left(\frac{\ell}{a}\right)^4 - 7682\left(\frac{\ell}{a}\right)^3 - 84850\left(\frac{\ell}{a}\right)^2 + 80940\left(\frac{\ell}{a}\right) - 97160}, & \text{if } \dfrac{\ell}{a} < 2, \\ \dfrac{\left(\frac{\ell}{a}\right)^3 + 3.606\left(\frac{\ell}{a}\right)^2 + 3.431\left(\frac{\ell}{a}\right) + 1.401}{\left(\frac{\ell}{a}\right)^3 - 3.219\left(\frac{\ell}{a}\right)^2 + 3.434\left(\frac{\ell}{a}\right) - 1.21}, & \text{if } \dfrac{\ell}{a} \geqslant 2. \end{cases} \tag{3.8}$$

(ii) Coupling shear flow and translating sphere:

$$L_{ST} = \begin{cases} \dfrac{-5.661\left(\frac{\ell}{a}\right)^5 - 179.4\left(\frac{\ell}{a}\right)^4 - 126.4\left(\frac{\ell}{a}\right)^3 + 704.5\left(\frac{\ell}{a}\right)^2 + 8.393\left(\frac{\ell}{a}\right) + 815.4}{\left(\frac{\ell}{a}\right)^4 + 32.18\left(\frac{\ell}{a}\right)^3 - 36.26\left(\frac{\ell}{a}\right)^2 + 10.58\left(\frac{\ell}{a}\right) - 124.8}, & \text{if } \dfrac{\ell}{a} < 2, \\ \dfrac{-9.288\left(\frac{\ell}{a}\right)^4 - 1.407\left(\frac{\ell}{a}\right)^3 + 3.606\left(\frac{\ell}{a}\right)^2 + 3.431\left(\frac{\ell}{a}\right) + 1.401}{\left(\frac{\ell}{a}\right)^4 + 1.902\left(\frac{\ell}{a}\right)^3 + 3.712\left(\frac{\ell}{a}\right)^2 + 0.9578\left(\frac{\ell}{a}\right) - 7.088}, & \text{if } \dfrac{\ell}{a} \geqslant 2. \end{cases} \tag{3.9}$$

(iii) Coupling quadratic flow and rotating sphere:

$$\frac{a}{\ell}L_{QR} = \begin{cases} \dfrac{0.1531\left(\dfrac{\ell}{a}\right)^4 + 4.047\left(\dfrac{\ell}{a}\right)^3 - 24.69\left(\dfrac{\ell}{a}\right)^2 + 46.47\left(\dfrac{\ell}{a}\right) - 29.11}{\left(\dfrac{\ell}{a}\right)^2 - 3.284\left(\dfrac{\ell}{a}\right) + 2.848}, & \text{if } \dfrac{\ell}{a} < 2, \\ \dfrac{2.487\left(\dfrac{\ell}{a}\right)^4 + 40.45\left(\dfrac{\ell}{a}\right)^3 - 75.38\left(\dfrac{\ell}{a}\right)^2 - 554.3\left(\dfrac{\ell}{a}\right) + 1065}{\left(\dfrac{\ell}{a}\right)^3 + 17.09\left(\dfrac{\ell}{a}\right)^2 - 42.96\left(\dfrac{\ell}{a}\right) - 47.53}, & \text{if } \dfrac{\ell}{a} \geqslant 2. \end{cases} \tag{3.8}$$

(iv) Coupling quadratic flow and translating sphere:

$$L_{QT} = \begin{cases} \dfrac{39.67\left(\dfrac{\ell}{a}\right)^4 - 319.9\left(\dfrac{\ell}{a}\right)^3 + 781.1\left(\dfrac{\ell}{a}\right)^2 - 766.8\left(\dfrac{\ell}{a}\right) + 266.2}{\left(\dfrac{\ell}{a}\right)^2 - 2.102\left(\dfrac{\ell}{a}\right) + 1.107}, & \text{if } \dfrac{\ell}{a} < 2, \\ \dfrac{-13.69\left(\dfrac{\ell}{a}\right)^4 - 443.2\left(\dfrac{\ell}{a}\right)^3 - 4288\left(\dfrac{\ell}{a}\right)^2 + 10840\left(\dfrac{\ell}{a}\right) - 7874}{\left(\dfrac{\ell}{a}\right)^2 + 62.63\left(\dfrac{\ell}{a}\right) - 33.03}, & \text{if } \dfrac{\ell}{a} \geqslant 2. \end{cases} \tag{3.9}$$

These formulae are valid for particle positions in the range $1.01 \leqslant \ell/a \leqslant 100$. Their relative error is below 2 %. These results will be applied in the next section.

4. Results for the migration velocity

Results of § 3 are exploited here to derive the migration velocity of an inertialess sphere in the case of no external force. The two cases of a sphere without rotation and of a freely rotating sphere will be considered: § 4.1 is concerned with a sphere moving in a linear shear flow and § 4.2 with a sphere immersed in a parabolic shear flow. We apply these results in § 4.3 to calculations of trajectories of an inertialess freely moving sphere in a parabolic shear flow near a wall.

For a Poiseuille flow (see figure 8), the maximum velocity is $V_m = H\tilde{K}_S/4 = -H^2\tilde{K}_Q/4$. We keep here the notation V_m and H to define the parabolic flow with one wall. Thereafter, the characteristic velocity for this type of geometry is given by

$$V'_\infty = \tilde{U}_p - \tilde{V}^\infty|_{z=\ell}.$$

In works on multiphase flows, V'_∞ is called a 'slip velocity'. For a sphere far from the

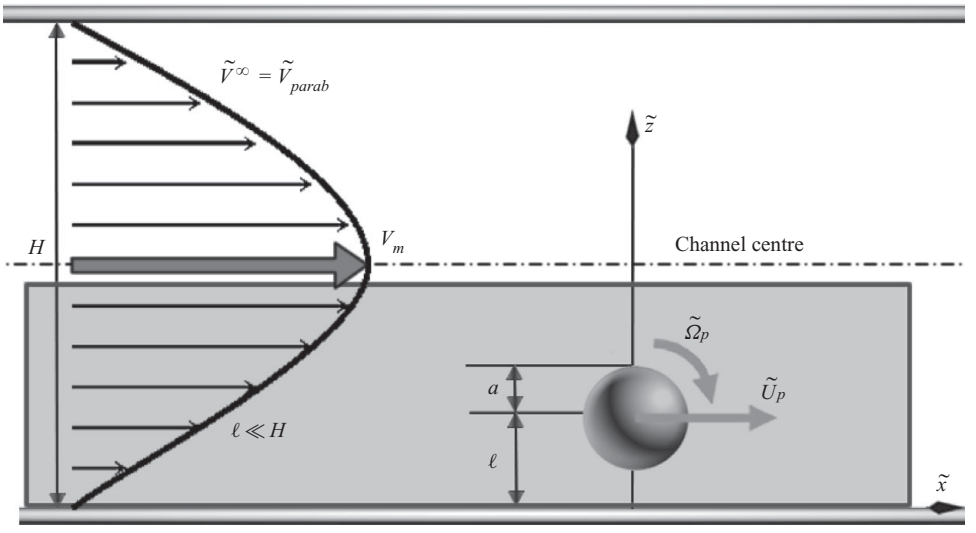

FIGURE 8. Particle moving in a parabolic flow near a wall. The domain of validity of our approach, $\ell \ll H$, is schematically represented in a grey shade.

wall, Cox & Hsu (1977) proposed an expression of the migration velocity for

(i) a sphere without rotation:

$$U_{pz}^{(1)} = \frac{3}{32}\frac{aV_\infty'^2}{\nu} - \frac{1}{32}\frac{aV_\infty' V_m}{\nu}\frac{\ell}{H}\left(22 - 105\frac{\ell}{H}\right) + \frac{1}{36}\frac{aV_m^2}{\nu}\frac{a^2}{\ell^2}\left(\frac{\ell}{H}\right)^2\left(1 - 2\frac{\ell}{H}\right)\left(61 - 368\frac{\ell}{H}\right), \quad (4.1)$$

(ii) a freely rotating sphere:

$$U_{pz}^{(1)} = \frac{3}{32}\frac{aV_\infty'^2}{\nu} - \frac{1}{32}\frac{aV_\infty' V_m}{\nu}\frac{\ell}{H}\left(22 - 105\frac{\ell}{H}\right) + \frac{5}{72}\frac{aV_m^2}{\nu}\frac{a^2}{\ell^2}\left(\frac{\ell}{H}\right)^2\left(1 - 2\frac{\ell}{H}\right)\left(22 - 146\frac{\ell}{H}\right). \quad (4.2)$$

The expressions (4.1) and (4.2), in principle valid for $a/\ell \ll 1$, contain three terms which were obtained for three separate cases by Cox & Hsu (1977), and they showed how to match the different cases. In the case $|V_\infty'/V_m| \sim 1$ with $a/\ell \ll 1$, they obtained the first two terms in (4.1) and (4.2), and, in the case $|V_\infty'/V_m| \ll (a/\ell)^2 \ll 1$, they found the last term in each equation. It is sufficient for our purpose, and even more precise, to take into account only the relevant terms of (4.1) and (4.2) in each specific case. We will extrapolate these results to smaller sphere-to-wall distances ($a/\ell \sim 1$), in order to assess their practical validity by comparing with our results.

4.1. *Migration of sphere in a linear shear flow*

In this subsection, we consider a moving sphere in a linear shear flow. The sphere is either non-rotating and translating with a prescribed velocity $\tilde{U}_p$ along $\tilde{x}$ (§ 4.1.1) or freely rotating and translating (§ 4.1.2).

4.1.1. *Translating and non-rotating sphere in a linear shear flow*

The migration velocity is given by the relationship (2.24) with (2.28), cancelling out terms due to a rotating sphere and a quadratic shear flow. For a better comparison

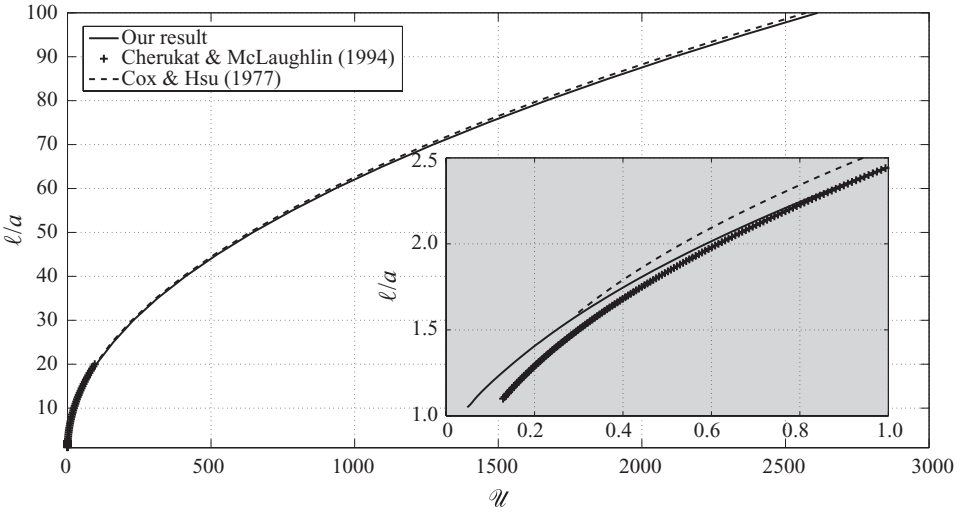

FIGURE 9. Normalized migration velocity $\mathscr{U}(\ell/a, 1)$ of a sphere with an imposed translation velocity $\tilde{U}_p = a\tilde{K}_S$ parallel to the wall and without rotation in a linear shear flow. The quantity $\mathscr{U}(\ell/a, 1)$ is represented versus ℓ/a. Our result (solid line) and comparison with the results of Cox & Hsu (1977) and Cherukat & McLaughlin (1994).

with the results of Cherukat & McLaughlin (1994), the expression for the dimensional migration velocity may be written as

$$\tilde{U}_{pz} = V^* Re U_{pz}^{(1)} = \frac{a\tilde{U}_p^2}{\nu_f} \mathscr{U}\left(\frac{\ell}{a}, \frac{a\tilde{K}_S}{\tilde{U}_p}\right), \tag{4.3}$$

with

$$\mathscr{U}\left(\frac{\ell}{a}, \frac{a\tilde{K}_S}{\tilde{U}_p}\right) = \frac{1}{6\pi D_z}\left\{L_T + \frac{a\tilde{K}_S}{\tilde{U}_p} L_{ST} + \left[\frac{a\tilde{K}_S}{\tilde{U}_p}\right]^2 L_S\right\}. \tag{4.4}$$

Here, we choose $V^* = a\tilde{K}_S$. For example, figure 9 represents (4.4) in the particular case $a\tilde{K}_S/\tilde{U}_p = 1$ for comparison with the results of Cherukat & McLaughlin (1994). Our results are close to theirs with a relative error of 10^{-2} in the range $2.3 \leqslant \ell/a \leqslant 20$. Our results are also close to the values of the velocity obtained by Cox & Hsu (1977) (with the first two terms in (4.1)). The 15 % difference at $\ell/a = 2.5$ decays for large ℓ/a to become of the order of a few per cent for $\ell/a = 100$. This difference may be understood since their formula is an approximation for large ℓ/a. Surprisingly, the result of Cox & Hsu (1977) again matches ours for $\ell/a = 1.5$ and below.

4.1.2. *A freely moving sphere in a linear shear flow*

For a freely translating and rotating sphere in a linear shear flow, the migration velocity is given by (2.24) with (2.28), cancelling out terms due to the quadratic flow. Similarly to (4.3) and (4.4), the dimensional migration velocity is written as follows:

$$\tilde{U}_{pz} = \frac{a\tilde{U}_p^2}{\nu_f} \mathscr{V}\left(\frac{\ell}{a}\right), \tag{4.5}$$

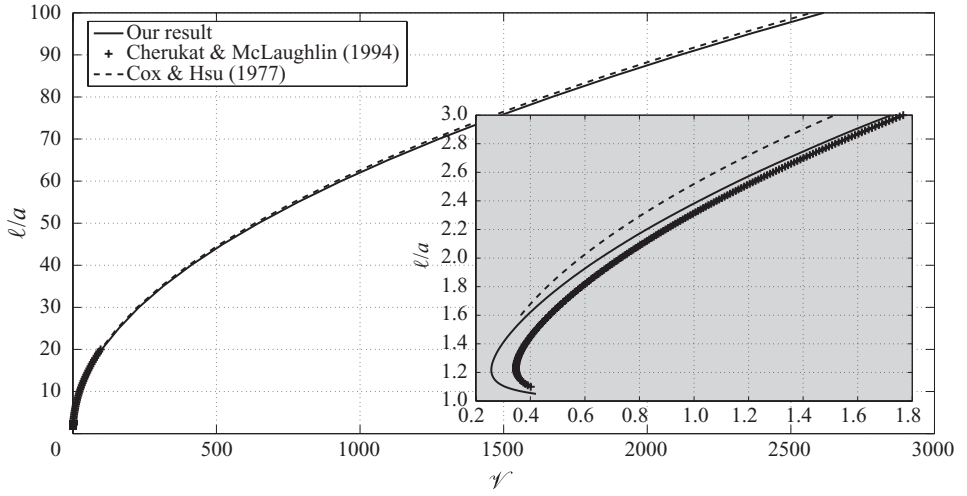

FIGURE 10. Normalized migration velocity $\mathscr{V}(\ell/a)$ of a freely translating and rotating sphere in a linear shear flow. The quantity $\mathscr{V}(\ell/a)$ is represented versus ℓ/a. This result (solid line) and comparison with the results of Cox & Hsu (1977) and Cherukat & McLaughlin (1994).

where

$$\mathscr{V}\left(\frac{\ell}{a}\right) = \frac{1}{6\pi D_z}\left\{L_T + \frac{a\tilde{K}_S}{\tilde{U}_p}\left[L_{ST} + \frac{\tilde{\Omega}_p}{\tilde{K}_S}L_{RT} + \frac{a\tilde{\Omega}_p}{\tilde{U}_p}L_{SR}\right] + \left[\frac{a\tilde{K}_S}{\tilde{U}_p}\right]^2\left[L_S + \left[\frac{\tilde{\Omega}_p}{\tilde{K}_S}\right]^2 L_R\right]\right\}, \quad (4.6)$$

by choosing $V^* = a\tilde{K}_S$. Here, the sphere dimensionless translational and rotational velocities are given by (2.16). The quantity $\mathscr{V}(\ell/a)$ is represented versus ℓ/a in figure 10 and compared with earlier results. The behaviour is similar to figure 9.

4.2. *Migration of a sphere in a parabolic flow*

In this subsection, we treat the cases of a non-rotating sphere translating with a prescribed velocity $\tilde{U}_p$ (§ 4.2.1) and of a freely moving sphere (§ 4.2.2). The ambient flow is parabolic, with velocity given by (2.1).

4.2.1. *Translating and non-rotating sphere in a parabolic shear flow*

The dimensional migration velocity of the non-rotating sphere translating with prescribed velocity $\tilde{U}_p$ along x may be written as

$$\tilde{U}_{pz} = \frac{a\tilde{U}_p^2}{\nu}\mathscr{W}\left(\frac{\ell}{H}, \frac{a}{H}, \frac{a\tilde{K}_S}{\tilde{U}_p}\right), \quad (4.7)$$

with

$$\mathscr{W}\left(\frac{\ell}{H}, \frac{a}{H}, \frac{a\tilde{K}_S}{\tilde{U}_p}\right) = \frac{1}{6\pi D_z}\left\{L_T + \frac{a\tilde{K}_S}{\tilde{U}_p}\left[L_{ST} - \frac{a}{H}L_{QT}\right] + \left[\frac{a\tilde{K}_S}{\tilde{U}_p}\right]^2\left[L_S - \frac{a}{H}L_{SQ} + \frac{a^2}{H^2}L_Q\right]\right\}, \quad (4.8)$$

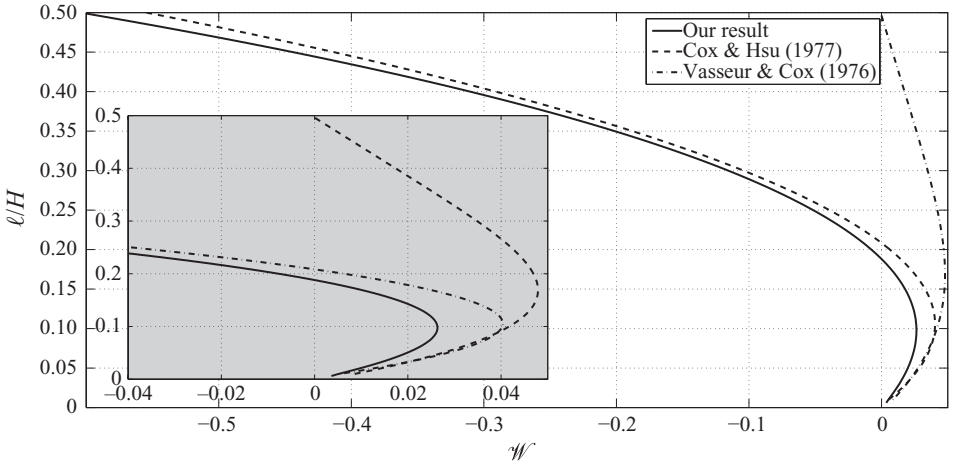

FIGURE 11. Normalized migration velocity $\mathscr{W}\left(\ell/H, a/H, a\tilde{K}_S/\tilde{U}_p\right)$ of a non-rotating sphere with an imposed translation velocity $\tilde{U}_p = a\tilde{K}_S$ in a parabolic flow $\tilde{V}^\infty = \tilde{K}_S\tilde{z} + \tilde{K}_Q\tilde{z}^2$ with $\tilde{K}_Q = -\tilde{K}_S/H$ in the example case $H/a = 200$, and comparison with the results of Cox & Hsu (1977) and Vasseur & Cox (1976).

by choosing $V^* = a\tilde{K}_S$. Figure 11 represents the normalized migration velocity (4.8) when the sphere-imposed translation velocity is $\tilde{U}_p = a\tilde{K}_S$; in the example case, $H/a = 200$. For a sphere coming in contact with the wall, $\ell/H \to a/H = 0.005$, the normalized migration velocity $\mathscr{W}$ is small but non-zero, as shown in the inset of figure 11. Our result is compared with that of Cox & Hsu (1977) (the first two terms in (4.1)). It is close to theirs at large distances, as it should since their assumption is $a/\ell \ll 1$. Again here, the small difference of the order of a few per cent may be due to their formula being an approximation for large ℓ/a. The difference increases at smaller distances, as shown in the inset, but both results match at $\ell/H \to 0$, a surprising result. It is observed that the migration velocity goes through zero, so that there is an equilibrium position for a particle-to-wall distance close to $\ell/H = 0.193$. By comparison, Cox & Hsu (1977) find an equilibrium position located at $\ell/H = 0.209$. From the sign of the migration velocity, this equilibrium position is stable. It should be noted that this migration-velocity profile is exact for a single wall but, for a Poiseuille flow between two walls, it is only an approximation valid when $\ell/H \leqslant 0.1$. Indeed, as observed in figure 11, the migration velocity for two walls obtained by Vasseur & Cox (1976) differs widely from the one for a single wall when $\ell/H > 0.1$.

4.2.2. *A freely moving sphere in a parabolic shear flow*

The expression of the dimensional migration velocity then is written as

$$\tilde{U}_{pz} = \frac{a\tilde{U}_p^{\,2}}{\nu_f}\,\mathscr{X}\left(\frac{\ell}{H}, \frac{a}{H}\right), \tag{4.9}$$

where

$$\mathscr{X}\left(\frac{\ell}{H}, \frac{a}{H}\right) = \frac{1}{6\pi D_z}\left\{L_T + \frac{a\tilde{K}_S}{\tilde{U}_p}\left[L_{CT} + \frac{\tilde{\Omega}_p}{\tilde{K}_S}L_{RT} + \frac{a\tilde{\Omega}_p}{\tilde{U}_p}L_{SR} - \frac{a}{H}L_{QT}\right.\right.$$
$$\left.\left. - \frac{a}{H}\frac{a\tilde{\Omega}_p}{\tilde{U}_p}L_{QR}\right] + \left[\frac{a\tilde{K}_S}{\tilde{U}_p}\right]^2\left[L_S + \left[\frac{a}{H}\right]^2 L_Q - \frac{a}{H}L_{SQ} + \left[\frac{\tilde{\Omega}_p}{\tilde{K}_S}\right]^2 L_R\right]\right\}, \tag{4.10}$$

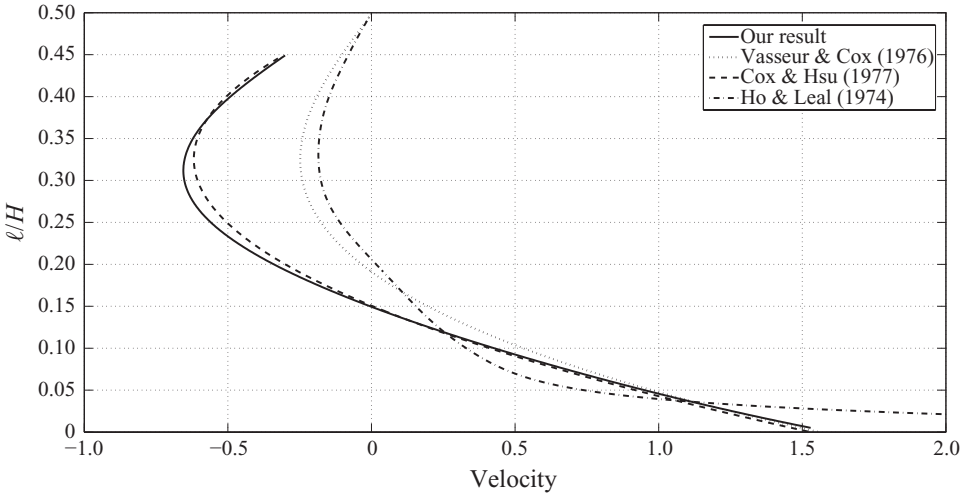

FIGURE 12. Normalized migration velocity $(H/a)^2(\tilde{U}_{pz}/V_m)^2\mathscr{X}(\ell/H, a/H)$ of a freely moving sphere in a parabolic flow (in the example case $H/a = 200$) and comparison with the results of Ho & Leal (1974), Vasseur & Cox (1976) and Cox & Hsu (1977).

by choosing $V^* = a\tilde{K}_S$. Here, the translational and rotational velocities of a freely rotating and translating sphere in a parabolic shear flow are given by (2.18) with (2.16) and (2.17).

The result of (4.10) is presented in figure 12 and compared with those of Cox & Hsu (1977) (the last term in (4.2)) and Vasseur & Cox (1976). We use here the normalization of figure 8 of Vasseur & Cox (1976) and represent $(H/a)^2(\tilde{U}_{pz}/V_m)^2\mathscr{X}(\ell/H, a/H)$ versus ℓ/H, taking as an example $H/a = 200$.

As in figure 11, our result is close to that of Cox & Hsu (1977), within a few per cent error at large distances. Both results again surprisingly match at small distances for which there is a non-zero migration velocity. Our results show a stable equilibrium position for $\ell/H = 0.149$. As displayed in the figure, this position is very close to the value $\ell/H = 11/73 \simeq 0.1507$ obtained by Cox & Hsu (1977).

Our results for the near-wall region are also consistent with figure 8 of Vasseur & Cox (1976). At large distances, the influence of the other wall considered by these authors gives a quite different equilibrium position. Note for the case when the wall is in the outer region, the result by Asmolov (1999) for a channel Reynolds number of 15 is close to the result of Vasseur & Cox (1976) for the case when the wall is in the inner region (our case), surprisingly even for small ℓ/H. Thus, our results are also close to those data of Asmolov (1999) for small ℓ/H.

4.3. *Trajectories of a freely moving sphere in a parabolic shear flow*

Using the previous calculations of the migration velocity (4.9) and axial velocity (2.16) and (2.17), we calculate the trajectories followed by an inertialess freely translating and rotating sphere in a parabolic flow limited by one wall. The conditions for particle inertia to be neglected are discussed in § 2.3, after (2.24); this is the case for a particle in a liquid.

Combining (4.9), (2.16) and (2.17), the differential equation for the trajectories (ℓ/H versus $\tilde{x}/H$ or ℓ/a versus $\tilde{x}/a$, where $\tilde{x}$ is the axial position of the

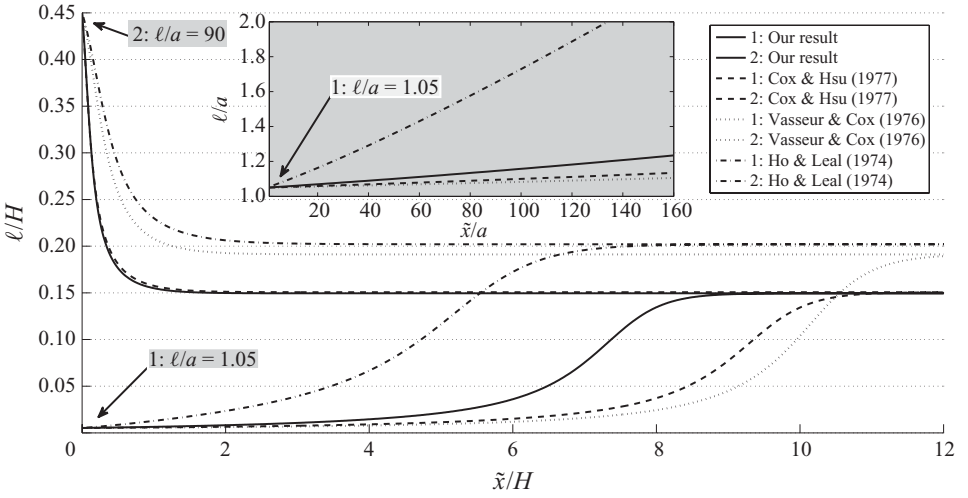

FIGURE 13. Trajectories of a freely moving sphere in a parabolic flow with $H/a = 200$.

sphere) is

$$\frac{\partial \ell}{\partial \tilde{x}} = \frac{\partial \ell}{\partial \tilde{t}} \cdot \frac{\partial \tilde{t}}{\partial \tilde{x}} = \frac{\tilde{U}_{pz}}{\tilde{U}_p} = \frac{a\tilde{U}_p}{\nu_f} \mathscr{X}\left(\frac{\ell}{H}, \frac{a}{H}\right), \tag{4.11}$$

where $\tilde{t}$ is the time. This equation was solved numerically for some initial positions $(\ell/a)_{x=0} = (\ell/a)_0$ and for $H = 200a$. The results are shown in figure 13 (solid lines) for $(\ell/a)_0 = 1.05$ and 90. Note that, particle inertia being negligible, the two displayed trajectories are 'universal' in the sense that any point on a trajectory could be considered as a starting position. The trajectories are monotonically converging to an equilibrium position. There is no oscillation around this asymptote because particle inertia is negligible. The final equilibrium position is for $\ell/a = 29.8$ corresponding to $\ell/H = 0.149$, as found in § 4.2.2. Particles leaving from the position close to the wall at $(\ell/a)_0 = 1.05$ reach the equilibrium position after a distance of around $9H$. The departure from a position near the wall is quite slow since it takes typically 160 radii for a particle to move a 0.2 radii away from the wall (see inset of figure 13). This remark may be relevant for the FFF separation technique in analytical chemistry, in which particles to be separated are released near a wall.

Our results are compared in figure 13 with those of Cox & Hsu (1977) (dashed lines), Vasseur & Cox (1976) (dotted lines) and Ho & Leal (1974) (dashed–dotted lines). For the slow departure from a wall (inset in figure 13), results are quite different and the importance of our precise account of particle–wall interactions is emphasized here. The final equilibrium position for one wall obtained from our calculation is the same as that of Cox & Hsu (1977). The time it takes to reach this position is practically the same if the particle is leaving from $\ell/a = 90$ but it is quite different if the particle is leaving from a position near the wall, at $\ell/a = 1.05$.

In the case of two walls, results of Vasseur & Cox (1976) provide the best approximation in the centre of the channel. For practical applications in the case of two walls, for a better precision our formula for a particle close to one wall could be combined with those of Vasseur & Cox (1976) valid for particles far away from two walls.

For a horizontal ambient flow, the weight of the particle may be taken into account by superimposing it to the lift force without modification. As explained in § 2.3, this superposition approximation is valid provided both forces are of the same order.

5. Conclusion and discussion

This paper is concerned with an inertialess spherical particle moving parallel to a wall in an ambient flow. Here, it appears that the particle is inertialess when its density is of the order of the fluid density, or less, as explained in the discussion following (2.24). The present analysis is limited to motions perpendicular to the wall being of second order in the Reynolds number. The results for the particle migration perpendicular to the wall appear in a quantity L and are interpreted either in terms of a lift force (see (2.23)) or in terms of a migration velocity for a freely moving sphere (see (2.24)). The 10 terms of L (see (2.28)) involve the sphere translation and rotation, the linear and quadratic parts of the shear flow and all binary couplings. They are obtained precisely for a large range of sphere-to-wall gaps down to 0.01 of a sphere radius (see table 1). These results for small gaps needed accurate calculations with a large number of digits, based on earlier accurate results of a creeping flow. The calculation required an increasingly larger time for smaller gaps; the lowest gap value of 0.01 considered here is usually sufficient in practice. The various results for the lift force are also displayed as figures and match with earlier results whenever available. Handy fitting formulae are provided in view of applications. Results for the migration velocity of a freely translating sphere are also given explicitly, for a non-rotating sphere with a prescribed translation velocity and for a freely moving sphere, the sphere being entrained by a parabolic shear flow. Here also, our results match with earlier ones. Typical particle trajectories are shown as examples. The importance of the near-wall hydrodynamic interactions is emphasized by the long time it takes for a particle to escape this near-wall region.

In this presentation, we did not consider any external supplementary force or torque acting on the particle. However, such forces might be relevant in applications and a discussion is appropriate. As explained above, the present analysis is limited to motions perpendicular to the wall being of second order in the Reynolds number. Otherwise, some supplementary coupling terms due to fluid inertia would arise. Thus, we exclude here a force perpendicular to the wall that would give a sphere velocity of the same order as the motion along the wall. However, this analysis allows for a small force perpendicular to the wall, of the same order as the lift due to fluid inertia. For a force along the wall, any force may be applied since its effect is embedded in the case of the arbitrary sphere motion along the wall. For the same reason as for the force perpendicular to the wall, any external torque considered here should be small, giving at most velocities of the order of the migration velocity.

A typical example of application is the FFF technique in analytical chemistry. There is usually another external force (either the gravity force in a horizontal channel or some other body force) of the same order as the lift force. Particles are assumed to be freely rotating. Since the external force and the lift force are of the same order, any coupling between their effects would be of third order and thus negligible. It is then a simple matter to add up the effects of these two forces so as to find the trajectories of particles. As compared with figure 13, the balance of both forces will change the final equilibrium position of the particle. This is how the FFF separation technique works: particles eventually reach some limiting streamline which depends on their size and are separated therefrom. A question which arises in FFF is the lift

force at start-up, when particles are close to one wall. This problem is resolved here, allowing us to determine the transient motion of particles. Thus, our calculation will allow us to refine the length of the channel necessary for separation. In this sense, the results presented here provide a contribution to the improvement of modelling of such separation techniques and are intended primarily to be compared with experiments.

Appendix A. Solutions of the Stokes flows

The solution of the Stokes momentum equation (2.7) for the pressure p and velocity (v_ρ, v_ϕ, v_z) is searched for in the following form:

$$p^\bullet = c^{M-1} Q_1^\bullet \cos\phi, \quad v_\rho^\bullet = \frac{1}{2} c^M \left(\frac{\rho}{c} Q_1^\bullet + \left(U_2^\bullet + U_0^\bullet \right) \right) \cos\phi, \tag{A 1a}$$

$$v_\phi^\bullet = \frac{1}{2} c^M \left(U_2^\bullet - U_0^\bullet \right) \sin\phi, \quad v_z^\bullet = \frac{1}{2} c^M \left(\frac{z}{c} Q_1^\bullet + 2 W_1^\bullet \right) \cos\phi, \tag{A 1b}$$

where

$$W_1^\bullet = (\cosh\xi - \mu)^{1/2} \sin\eta \sum_{n=1}^{\infty} \left[0, A_n^\bullet \right] P_n'(\mu), \tag{A 2a}$$

$$Q_1^\bullet = (\cosh\xi - \mu)^{1/2} \sin\eta \sum_{n=1}^{\infty} \left[B_n^\bullet, C_n^\bullet \right] P_n'(\mu), \tag{A 2b}$$

$$U_0^\bullet = (\cosh\xi - \mu)^{1/2} \sum_{n=0}^{\infty} \left[D_n^\bullet, E_n^\bullet \right] P_n(\mu), \tag{A 2c}$$

$$U_2^\bullet = (\cosh\xi - \mu)^{1/2} \sin^2\eta \sum_{n=2}^{\infty} \left[F_n^\bullet, G_n^\bullet \right] P_n''(\mu). \tag{A 2d}$$

The symbol ($^\bullet$) represents any of the letters T, R, S and Q, which correspond to the four basic flows: translation ($M=0$), rotation ($M=1$), linear shear flow ($M=1$) and quadratic shear flow ($M=2$). Here, $\mu = \cos\eta$, P_n is the Legendre polynomial of order n and $P_n'(\mu)$ (respectively $P_n''(\mu)$) is given by $\partial P_n(\mu)/\partial\mu$ (respectively $\partial^2 P_n(\mu)/\partial\mu^2$). We also used the shorthand notation:

$$\left[B_{\boldsymbol{n}}^\bullet, C_{\boldsymbol{n}}^\bullet \right] = B_{\boldsymbol{n}}^\bullet \cosh\left(n + \tfrac{1}{2}\right)\xi + C_{\boldsymbol{n}}^\bullet \sinh\left(n + \tfrac{1}{2}\right)\xi. \tag{A 3}$$

The velocity satisfies the no-slip condition on the wall. It also vanishes at infinity since $\xi = \eta = 0$ there. Then applying the no-slip boundary condition on the sphere surface, the coefficients $B_n^\bullet, C_n^\bullet, C_n^\bullet, D_n^\bullet, E_n^\bullet, F_n^\bullet$ are expressed in terms of the $A_n^\bullet$ (see, e.g., Chaoui & Feuillebois 2003). An appropriate solution using an iterative technique was proposed by O'Neill & Bhatt (1991) and applied by Chaoui & Feuillebois (2003) using high-precision arithmetic. The linear shear flow $\tilde{V}_x^\infty = \tilde{K}_S \tilde{z}$ was considered in their article and the quadratic shear flow $\tilde{V}_x^\infty = \tilde{K}_Q \tilde{z}^2$ in Pasol *et al.* (2006).

Appendix B. Details of calculation of the lift force

B.1. *Velocity gradients*

Here, we calculate the velocity gradients in bispherical coordinates appearing in (2.28) for the lift force. The components of the gradient of the $\boldsymbol{v}_S, \boldsymbol{v}_Q, \boldsymbol{v}_T, \boldsymbol{v}_R, \boldsymbol{V}_S^\infty, \boldsymbol{V}_Q^\infty$

velocities, i.e. $\nabla \boldsymbol{v}_\bullet$ and $\nabla \boldsymbol{V}_\bullet^\infty$, may be written as a matrix $\boldsymbol{G}^\bullet$:

$$\boldsymbol{G}^\bullet = \begin{bmatrix} g^\bullet_{\eta\eta}\cos\phi & g^\bullet_{\eta\xi}\cos\phi & g^\bullet_{\eta\phi}\sin\phi \\ g^\bullet_{\xi\eta}\cos\phi & g^\bullet_{\xi\xi}\cos\phi & g^\bullet_{\xi\phi}\sin\phi \\ g^\bullet_{\phi\eta}\sin\phi & g^\bullet_{\phi\xi}\sin\phi & g^\bullet_{\phi\phi}\cos\phi \end{bmatrix}. \tag{B 1}$$

B.1.1. *Perturbed flows*

Using the expressions of the perturbed velocities in bispherical coordinates (see Appendix A):

$$v^\bullet_\eta = \frac{\cosh\xi - \cos\eta}{c}\left[v^\bullet_\rho \frac{\partial\rho}{\partial\eta} + v^\bullet_z \frac{\partial z}{\partial\eta}\right] = h^\bullet_\eta \cos\phi, \tag{B 2}$$

$$v^\bullet_\xi = \frac{\cosh\xi - \cos\eta}{c}\left[v^\bullet_\rho \frac{\partial\rho}{\partial\xi} + v^\bullet_z \frac{\partial z}{\partial\xi}\right] = h^\bullet_\xi \cos\phi, \tag{B 3}$$

$$v^\bullet_\phi = h^\bullet_\phi \sin\phi, \tag{B 4}$$

with the expressions for $h^\bullet_\eta$, $h^\bullet_\xi$ and $h^\bullet_\phi$ in bispherical coordinates:

$$h^\bullet_\eta = \frac{1}{2}c^M\left[\frac{(\cosh\xi\cos\eta - 1)(U^\bullet_2 + U^\bullet_0) - \cosh\xi\sin\eta Q^\bullet_1 - 2\sinh\xi\sin\eta W^\bullet_1}{\cosh\xi - \cos\eta}\right], \tag{B 5}$$

$$h^\bullet_\xi = -\frac{1}{2}c^M\left[\frac{(\sinh\xi\sin\eta(U^\bullet_2 + U^\bullet_0) + \sinh\xi\cos\eta Q^\bullet_1 + 2(\cos\eta\cosh\xi - 1)W^\bullet_1}{\cosh\xi - \cos\eta}\right], \tag{B 6}$$

$$h^\bullet_\phi = \frac{1}{2}c^M\left[U^\bullet_2 - U^\bullet_0\right], \tag{B 7}$$

the components of the velocity gradient are:

$$g^\bullet_{\eta\eta} = \frac{1}{2}c^{M-1}\left[(\cosh\xi\cos\eta - 1)\left(\frac{\partial U^\bullet_2}{\partial\eta} + \frac{\partial U^\bullet_0}{\partial\eta}\right) + Q^\bullet_1 - \cosh\xi\sin\eta\frac{\partial Q^\bullet_1}{\partial\eta} - 2\sinh\xi\sin\eta\frac{\partial W^\bullet_1}{\partial\eta}\right], \tag{B 8}$$

$$g^\bullet_{\eta\xi} = -\frac{1}{2}c^{M-1}\left[\sinh\xi\sin\eta\left(\frac{\partial U^\bullet_2}{\partial\eta} + \frac{\partial U^\bullet_0}{\partial\eta}\right) + \sinh\xi\cos\eta\frac{\partial Q^\bullet_1}{\partial\eta} + 2(\cosh\xi\cos\eta - 1)\frac{\partial W^\bullet_1}{\partial\eta}\right], \tag{B 9}$$

$$g^\bullet_{\eta\phi} = \frac{1}{2}c^{M-1}(\cosh\xi - \cos\eta)\left(\frac{\partial U^\bullet_2}{\partial\eta} - \frac{\partial U^\bullet_0}{\partial\eta}\right), \tag{B 10}$$

$$g^\bullet_{\xi\eta} = \frac{1}{2}c^{M-1}\left[(\cosh\xi\cos\eta - 1)\left(\frac{\partial U^\bullet_2}{\partial\xi} + \frac{\partial U^\bullet_0}{\partial\xi}\right) - \cosh\xi\sin\eta\frac{\partial Q^\bullet_1}{\partial\xi} - 2\sinh\xi\sin\eta\frac{\partial W^\bullet_1}{\partial\xi}\right], \tag{B 11}$$

$$g^\bullet_{\xi\xi} = -\frac{1}{2}c^{M-1}\left[\sinh\xi\sin\eta\left(\frac{\partial U^\bullet_2}{\partial\xi} + \frac{\partial U^\bullet_0}{\partial\xi}\right) - Q^\bullet_1 + \sinh\xi\cos\eta\frac{\partial Q^\bullet_1}{\partial\xi} + 2(\cosh\xi\cos\eta - 1)\frac{\partial W^\bullet_1}{\partial\xi}\right], \tag{B 12}$$

$$g^{\bullet}_{\xi\phi} = \frac{1}{2}c^{M-1}(\cosh\xi - \cos\eta)\left(\frac{\partial U_2^{\bullet}}{\partial \xi} - \frac{\partial U_0^{\bullet}}{\partial \xi}\right), \tag{B 13}$$

$$g^{\bullet}_{\phi\eta} = -\frac{1}{2}c^{M-1}\frac{2(\cosh\xi\cos\eta - 1)U_2^{\bullet} - \cosh\xi\sin\eta Q_1^{\bullet} - 2\sin\eta\sinh\xi W_1^{\bullet}}{\sin\eta}, \tag{B 14}$$

$$g^{\bullet}_{\phi\xi} = \frac{1}{2}c^{M-1}\frac{2\sin\eta\sinh\xi U_2^{\bullet} + \sinh\xi\cos\eta Q_1^{\bullet} + 2(\cosh\xi\cos\eta - 1)W_1^{\bullet}}{\sin\eta}, \tag{B 15}$$

$$g^{\bullet}_{\phi\phi} = \frac{1}{2}c^{M-1}\frac{2(\cosh\xi - \cos\eta)U_2^{\bullet} + \sin\eta Q_1^{\bullet}}{\sin\eta}. \tag{B 16}$$

B.1.2. *Unperturbed linear and quadratic shear flows*

The components of the gradient of the unperturbed linear shear flow velocity $\nabla \boldsymbol{V}_S^{\infty}$ are expressed as

$$g^{S\infty}_{\eta\eta} = -\frac{\sin\eta\sinh\xi(\cos\eta\cosh\xi - 1)}{(\cosh\xi - \cos\eta)^2}, \tag{B 17}$$

$$g^{S\infty}_{\eta\xi} = -\frac{(1-\cos\eta^2)(1-\cosh\xi^2)}{(\cosh\xi - \cos\eta)^2}, \tag{B 18}$$

$$g^{S\infty}_{\eta\phi} = \frac{\sin\eta\sinh\xi}{\cosh\xi - \cos\eta}, \tag{B 19}$$

$$g^{S\infty}_{\xi\eta} = -\left[\frac{\cos\eta\cosh\xi - 1}{\cosh\xi - \cos\eta}\right]^2, \tag{B 20}$$

$$g^{S\infty}_{\xi\xi} = \frac{\sin\eta\sinh\xi(\cos\eta\cosh\xi - 1)}{(\cosh\xi - \cos\eta)^2}, \tag{B 21}$$

$$g^{S\infty}_{\xi\phi} = \frac{\cos\eta\cosh\xi - 1}{\cosh\xi - \cos\eta}, \tag{B 22}$$

$$g^{S\infty}_{\phi\eta} = g^{S\infty}_{\phi\xi} = g^{S\infty}_{\phi\phi} = 0. \tag{B 23}$$

For the unperturbed quadratic shear flow, we have

$$g^{Q\infty}_{\eta\eta} = -2c\frac{(\cosh^2\xi - 1)(\cos\eta\cosh\xi - 1)\sin\eta}{(\cosh\xi - \cos\eta)^3}, \tag{B 24}$$

$$g^{Q\infty}_{\eta\xi} = -2c\frac{(\cosh^2\xi - 1)(\cos\eta\cosh\xi - 1)\sinh\xi}{(\cosh\xi - \cos\eta)^2}, \tag{B 25}$$

$$g^{Q\infty}_{\eta\phi} = 2c\frac{(\cosh^2\xi - 1)\sin\eta}{(\cosh\xi - \cos\eta)^2}, \tag{B 26}$$

$$g^{Q\infty}_{\xi\eta} = -2c\frac{(\cos\eta\cosh\xi - 1)^2\sinh\xi}{(\cosh\xi - \cos\eta)^3}, \tag{B 27}$$

$$g^{Q\infty}_{\xi\xi} = 2c\frac{(\cosh^2\xi - 1)(\cos\eta\cosh\xi - 1)\sin\eta}{(\cosh\xi - \cos\eta)^3}, \tag{B 28}$$

$$g^{Q\infty}_{\xi\phi} = 2c\frac{(\cos\eta\cosh\xi - 1)\sinh\xi}{\cosh\xi - \cos\eta}, \tag{B 29}$$

$$g^{Q\infty}_{\phi\eta} = g^{Q\infty}_{\phi\xi} = g^{Q\infty}_{\phi\phi} = 0. \tag{B 30}$$

ε	0.1	1	2	5	10	99
C_1^S	19.99375	3.21560	2.32739	1.84020	1.70156	1.60019
C_2^S	35.29968	2.22142	1.35978	0.96086	0.86238	0.80023
C_1^Q	32.35269	7.69521	7.69207	11.36900	18.89371	161.63892
C_2^Q	65.19162	5.81405	4.75907	6.05659	9.64022	80.84004
C_1^R	−4.80727	−0.34840	−0.13188	−0.03028	−0.00884	0.00010
C_2^R	−12.00081	−0.40590	−0.14029	−0.03072	−0.00887	0.00010
C_1^T	−13.60523	−1.41229	−0.72399	−0.30038	−0.15365	−0.01584
C_2^T	−18.36594	−0.85731	−0.39418	−0.15352	−0.07734	−0.00792

TABLE 2. Values of the coefficients appearing in (C1) versus the dimensionless gap ε.

B.2. *An example of integral for the lift force*

Using the preceding results, we obtain, for example, the lift term in (2.28) for a purely rotating sphere:

$$L_R = \int_0^{\pi}\int_0^{\alpha}\int_0^{2\pi}\Big[\frac{w_\eta}{2}\left\{h_\eta^R g_{\eta\eta}^R + h_\xi^R g_{\xi\eta}^R + h_\phi^R g_{\phi\eta}^R\right\} + \frac{w_\xi}{2}\left\{h_\eta^R g_{\eta\xi}^R + h_\xi^R g_{\xi\xi}^R + h_\phi^R g_{\phi\xi}^R\right\} + C_R(\eta,\xi)\cos 2\phi\Big]\,\mathrm{d}\eta\,\mathrm{d}\xi\,\mathrm{d}\phi. \quad \text{(B 31)}$$

The coefficients w_η and w_ξ correspond to the components of the velocity field $\boldsymbol{w}$ in a Stokes flow for a sphere moving normal to the wall with a unit velocity. Details are given in Yahiaoui (2008). It may be noted that the integral of the $C_R(\eta,\xi)\cos 2\phi$ term for ϕ in $[0, 2\pi]$ vanishes.

Appendix C. Expansions of the velocity fields far from the particle

Here, we discuss the asymptotic expansions of the velocities at infinity in the half-space fluid domain V_f, in order to quantify these quantities and estimate the decay of the integrand $\boldsymbol{f}\cdot\boldsymbol{w}$, giving convergent integrals for the lift force (2.28). The point at infinity in Cartesian or cylindrical coordinates corresponds to $\eta=\xi=0$ in bispherical coordinates. Far-field expansions are derived in terms of a small parameter $\delta \ll 1$, replacing (η,ξ) by $(\eta'\delta,\xi'\delta)$, where η' and ξ' are of order unity.

C.1. *The basic flow velocities*

The expansions of the basic flow velocities far from the particle were obtained using Maple™ symbolic calculus software. Results are detailed below.

(i) Velocities for the cases of rotation, translation, linear and quadratic shear flows are functions of $(h_\eta^\bullet, h_\xi^\bullet, h_\phi^\bullet)$, which have the following expansions:

$$h_\eta^\bullet \simeq C_1^\bullet\sqrt{2}\frac{\eta^2\xi'}{\sqrt{\eta'^2+\xi'^2}}\delta^2, \quad h_\xi^\bullet \simeq C_1^\bullet\sqrt{2}\frac{\eta'\xi'^2}{\sqrt{\eta'^2+\xi'^2}}\delta^2 \quad \text{and} \quad h_\phi^\bullet \simeq \frac{C_2^\bullet}{\sqrt{2}}\xi'^2\sqrt{\eta'^2+\xi'^2}\delta^3, \quad \text{(C 1)}$$

where the constants $C_1^\bullet$ and $C_2^\bullet$ are functions of the position $\varepsilon=\ell/a-1$; values are given for $0.1\leqslant\varepsilon\leqslant 99$ in table 2.

From the above results, the velocities $\boldsymbol{v}^{(0)}$ at infinity scale like δ^2, that is like $1/\|\boldsymbol{r}\|^2$.

ε	0.1	1	2	5	10	99
$C^{\perp}$	−29.55469	−1.15330	−0.48353	−0.16996	−0.08165	−0.00797

TABLE 3. Values of $C^{\perp}$ versus the dimensionless gap ε.

ε	0.1	1	2	5	10	99
C^{r}	0.91652	3.4641	5.6568	11.8321	21.9089	201.9901

TABLE 4. Values of C^{r} versus the dimensionless gap ε.

(ii) The velocity $\boldsymbol{w}$ in the case of sedimentation of the sphere perpendicular to the wall is a function of $h_{\eta}^{\perp}$ and $h_{\xi}^{\perp}$, which have the following expansions:

$$h_{\eta}^{\perp} \simeq \frac{C^{\perp}}{\sqrt{2}}\eta'\xi'\frac{\xi'^2 - 2\eta'^2}{\sqrt{\eta'^2+\xi'^2}}\delta^3, \quad h_{\xi}^{\perp} \simeq \frac{C^{\perp}}{\sqrt{2}}\xi'^2\frac{2\xi'^2 - \eta'^2}{\sqrt{\eta'^2+\xi'^2}}\delta^3, \tag{C 2}$$

where $C^{\perp}$ is given in table 3.

From the above results, the velocity $\boldsymbol{w}$ at infinity scales like δ^3, that is like $1/\|\boldsymbol{r}\|^3$. This is the result found by Blake (1971) for the behaviour of the fluid velocity at a large distance from a particle moving perpendicular to a wall in a fluid at rest.

C.2. *Expansion of the distance*

The distance from the origin to a point in the flow field is given by $\|\boldsymbol{r}\| = c\sqrt{(\cosh\xi + \cos\eta)/(\cosh\xi - \cos\eta)}$. Its expansion for small η and ξ is $\|\boldsymbol{r}\| \simeq C^{r}/(\delta\sqrt{\eta'^2+\xi'^2})$, where C^{r} is given in table 4.

C.3. *Convergence of the integral for the lift force*

We now study the convergence of the integral for the lift force in (2.23):

$$L = \int_{V_f} \boldsymbol{f}\cdot\boldsymbol{w}\,\mathrm{d}V, \tag{C 3}$$

with $\boldsymbol{f} = \boldsymbol{v}^{(0)}\cdot\nabla\boldsymbol{v}^{(0)} + \boldsymbol{v}^{(0)}\cdot\nabla\boldsymbol{V}^{\infty} + \boldsymbol{V}^{\infty}\cdot\nabla\boldsymbol{v}^{(0)} - \boldsymbol{U}_p^{(0)}\cdot\nabla\boldsymbol{v}^{(0)}$.

From the results of the preceding §§ C.1 and C.2, we have

$$\boldsymbol{v}^{(0)} \approx \frac{1}{\|\boldsymbol{r}\|^2}, \quad \boldsymbol{w} \approx \frac{1}{\|\boldsymbol{r}\|^3}, \quad \boldsymbol{U}_p^{(0)} = O(1), \quad \boldsymbol{V}_S^{\infty} \approx \|\boldsymbol{r}\|, \quad \boldsymbol{V}_Q^{\infty} \approx \|\boldsymbol{r}\|^2 \quad \text{and} \quad \nabla \approx \frac{1}{\|\boldsymbol{r}\|}. \tag{C 4}$$

Thus, $\boldsymbol{f}\cdot\boldsymbol{w} \approx 1/\|\boldsymbol{r}\|^4$ and the integral is convergent.

REFERENCES

ASMOLOV, E. S. 1999 The inertial lift on a spherical particle in a plane Poiseuille flow at large channel Reynolds number. *J. Fluid Mech.* **381**, 63–87.

BLAKE, J. R. 1971 A note on the image system for a Stokeslet in a no-slip boundary. *Proc. Camb. Phil. Soc.* **70**, 303–310.

BRENNER, H. 1961 The slow motion of a sphere through a viscous fluid towards a plane surface. *Chem. Engng Sci.* **16**, 242–251.

BRETHERTON, F. P. 1962 The motion of rigid particles in a shear flow at low Reynolds number. *J. Fluid Mech.* **14**, 284–304.

CHAOUI, M. & FEUILLEBOIS, F. 2003 Creeping flow around a sphere in a shear flow close to a wall. *Q. J. Mech. Appl. Maths* **56** (3), 381–410.

Cherukat, P. & McLaughlin, J. B. 1994 The inertial lift on a rigid sphere in a linear shear flow field near a flat wall. *J. Fluid Mech.* **263**, 1–18 (corrigendum: *J. Fluid Mech.* **285**, 407, 1995).

Cox, R. G. & Brenner, H. 1967 The slow motion of a sphere through a viscous fluid towards a plane surface. II: Small gap widths including inertial effects. *Chem. Engng Sci.* **22**, 1753–1777.

Cox, R. G. & Brenner, H. 1968 The lateral migration of solid particles in Poiseuille flow. *Chem. Engng Sci.* **23**, 147–173.

Cox, R. G. & Hsu, S. K. 1977 The lateral migration of solid particles in a laminar flow near a plane. *Intl J. Multiphase Flow* **3**, 201–222.

Feuillebois, F. 1989 Some theoretical results for the motion of solid spherical particles in a viscous fluid. In *Multiphase Science and Technology* (ed. G. F. Hewitt, J. M. Delhaye & N. Zuber), vol. 4, pp. 538–798. Hemisphere.

Feuillebois, F. 2004 *Perturbation Problems at Low Reynolds Number*. Lecture Notes of Center of Excellence of Advanced Materials and Structures, vol. 15. Polish Academy of Sciences.

Giddings, J. C. 1978 Displacement and dispersion of particles of finite size in flow channels with lateral forces. Field-flow-fractionation and hydrodynamic chromatography. *Separation Sci. Technol.* **13**, 241–254.

Happel, J. & Brenner, H. 1967 *Low Reynolds Number Hydrodynamics*. Kluwer.

Ho, B. P. & Leal, L. G. 1974 Inertial migration of rigid spheres in two-dimensional unidirectional flows. *J. Fluid Mech.* **65**, 365–400.

Krishnan, G. P. & Leighton, D. T. Jr. 1995 Inertial lift on a moving sphere in contact with a plane wall in a shear flow. *Phys. Fluids* **7** (11), 2538–2545.

Kythe, P. K. & Schferkotter, M. R. 2004 *Handbook of Computational Methods for Integration*. Chapman & Hall/CRC.

Legendre, D. & Magnaudet, J. 1997 A note on the lift force on a spherical bubble or drop in a low-Reynolds-number shear flow. *Phys. Fluids* **9** (11), 3472–3474.

Legendre, D. & Magnaudet, J. 1998 The lift force on a spherical bubble in a viscous linear shear flow. *J. Fluid Mech.* **368**, 81–126.

Leighton, D. & Acrivos, A. 1987 Measurement of shear-induced self-diffusion in concentrated suspensions of spheres. *J. Fluid Mech.* **177**, 109–131.

Magnaudet, J. 2003 Small inertial effects on a spherical bubble, drop or particle moving near a wall in a time-dependent linear flow. *J. Fluid Mech.* **485**, 115–142.

Maude, A. D. 1961 End effects in a falling-sphere viscometer. *Br. J. Appl. Phys.* **12**, 293–295.

O'Neill, M. E. 1964 A slow motion of viscous liquid caused by a slowly moving solid sphere. *Mathematika* **11**, 67–74.

O'Neill, M. E. & Bhatt, B. S. 1991 Slow motion of a solid sphere in the presence of a naturally permeable surface. *Q. J. Mech. Appl. Maths* **44**, 91–104.

Oseen, C. W. 1914 Ueber den gueltigkeitsbereich der stokesschen widerstandsformel. *Ark. Mat., Astron. Fys.* **9** (16), 1–15.

Pasol, L., Sellier, A. & Feuillebois, F. 2006 A sphere in a second degree polynomial creeping flow parallel to a wall. *Q. J. Mech. Appl. Maths* **59**, 587–614.

Proudman, I. & Pearson, J. R. A. 1957 Expansions at small Reynolds numbers for the flow past a sphere and a circular cylinder. *J. Fluid Mech.* **2**, 237–262.

Saffman, P. G. 1965 The lift on a small sphere in a slow shear flow. *J. Fluid Mech.* **22**, 385–400 (corrigendum: *J. Fluid Mech.* **31**, 624 (1968)).

Segré, G. & Silberberg, A. 1961 Radial particle displacements in Poiseuille flow of suspensions. *Nature* **189** (4760), 209–210.

Segré, G. & Silberberg, A. 1962*a* Behaviour of macroscopic rigid spheres in Poiseuille flow. *J. Fluid Mech.* **14**, 115–135.

Segré, G. & Silberberg, A. 1962*b* Behaviour of macroscopic rigid spheres in Poiseuille flow. *J. Fluid Mech.* **14**, 136–157.

Tözeren, H. & Skalak, R. 1977 Stress in a suspension near rigid boundaries. *J. Fluid Mech.* **82**, 289–307.

Vasseur, P. & Cox, R. G. 1976 The lateral migration of a spherical particle in two-dimensional shear flows. *J. Fluid Mech.* **78**, 385–413.

Yahiaoui, S. 2008 Transport de petites particules par un écoulement de fluide visqueux. PhD thesis, Université Pierre et Marie Curie – Paris 6.